DE GRUYTER Open Physics 2024; 22: 20240084

Research Article

Kiran Sajjan, Chakravarthula Siva Krishnam Raju, Mansoor Alshehri, and Nehad Ali Shah*

Homotopic dynamic solution of hydrodynamic nonlinear natural convection containing superhydrophobicity and isothermally heated parallel plate with hybrid nanoparticles

https://doi.org/10.1515/phys-2024-0084
received February 06, 2024; accepted August 10, 2024

Abstract: The purpose of this work is to investigate the effect of thermal radiation on convective heat transfer for an electrically conducting hybrid nanofluid moving perpendicularly through a microchannel with parallel plates heated under isothermal conditions, while subjected to a transverse magnetic field. In this case, one surface exhibited a superhydrophobic slip and temperature jump, whereas the others did not. The objective of the study was to determine the impacts of thermal radiation, heat generation, and magnetism on the volume flow rate, velocity, and bulk temperature when either surface is heated by a constant wall temperature. Our findings reveal that the radiation parameter significantly influences both the Nusselt number and skin friction differently depending on the surface conditions, while also reducing flow rate and bulk temperature. The heat generation parameter similarly affects these variables but varies with the type of surface being heated. Additionally, both the velocity and temperature profiles increase with the porosity parameter and heat generation coefficient, regardless of the heated surface. Statistical analysis confirms the significance of magnetic and heat generation parameters in determining skin friction and the Nusselt number, and streamlines and isotherms illustrating the effects of thermal radiation and magnetism on two different hybrid nanofluids when heated on nonslip and superhydrophobic surfaces were provided. These insights provide valuable information for the design and maintenance of mini- and microdevices in the fields of nanoscience and nanotechnology.

Keywords: temperature jump, superhydrophobic slip, microchannel, hybrid nanofluid, vertical slit, MHD, nanofluid, nonlinear Boussinesq approximation, thermal radiation, heat generation/absorption

Nomenclature

Symbols

y	Cartesian coordinate in the flow direction (m)
T	fluid temperature (K)
Y	dimensionless Cartesian coordinate (−)
R	thermal radiation
Q_T	heat generation/absorption
T_0	surrounding temperature (K)
B_0	magnetic field (T)
Q_0	internal heat generation constant ($\mathrm{W\,K^{-1}}$)
Ec	Eckert number
Pr	Prandtl number
Kp	porosity parameter
U	dimensionless upward velocity (−)
B	magnetic field vector (T)
NSS	no-slip surface
SHS	superhydrophobic surface
M	magnetic parameter (−)
N	NDT parameter (nonlinear density variation with temperature) (−)
u	dimensional upward flow velocity ($\mathrm{m\,s^{-1}}$)
$\vec{F}$	magnetic Lorentz force (T)

*** Corresponding author: Nehad Ali Shah,** Department of Mechanical Engineering, Sejong University, Seoul, 05006, Republic of Korea, e-mail: nehadali199@sejong.ac.kr
Kiran Sajjan: Department of Mathematics, GITAM School of Science, GITAM Deemed to be University, Bangalore-Campus, Bengaluru, Karnataka, 562163, India, e-mail: kiransajjan5@gmail.com
Chakravarthula Siva Krishnam Raju: RTA Centre for Science Innovation, School of Computer Science and Engineering, RV University, Bengaluru, Karnataka, 560059, India, e-mail: chakravarthulask@rvu.edu.in, sivapdf90@gmail.com
Mansoor Alshehri: Department of Mathematics, College of Sciences, King Saud University, P.O. Box 2455, Riyadh, 11451, Saudi Arabia, e-mail: mhalshehri@ksu.edu.sa

k^*	Rosseland mean absorption coefficient
Nu	Nusselt number (−)
V	velocity vector field ($\mathrm{m\,s^{-1}}$)
T_w	wall temperature (K)
L	channel width (m)
$\vec{E}$	electric field force ($\mathrm{N\,C^{-1}}$ or $\mathrm{V\,m^{-1}}$)
$\vec{B}$	transverse magnetic field vector (T)
$\vec{J}$	current density

Greek letters

γ' and γ	dimensional and dimensionless temperature jump
θ	dimensionless temperature (−)
Q	non-dimensional volume flow rate (−)
λ	dimensionless slip length (−)
β_1	fluid's second-degree thermal expansion coefficient ($\mathrm{K^{-2}}$)
λ'	dimensional slip length (m)
ρ_hnf	hybrid nanofluid's density ($\mathrm{kg\,m^{-3}}$)
θ_b	bulk temperature (−)
σ_hnf	hybrid nanofluid's electrical conductivity ($\mathrm{A^2\,s^3\,kg^{-1}\,m^{-3}}$)
ϕ_1 & ϕ_2	volume fraction of the nanofluids
$(\beta_0)_\mathrm{f}$	initial thermal expansion coefficient ($\mathrm{K^{-1}}$)
ν_hnf	hybrid nanofluid's kinematic viscosity ($\mathrm{m^2\,s^{-1}}$)
μ_hnf	hybrid nanofluid's viscosity ($\mathrm{N\,s\,m^{-2}}$)
σ^*	Stefan–Boltzmann constant

1 Introduction

Scientists are now looking for ways to enhance heat transmission in heat exchangers and other industrial equipment as a result of recent improvements in the industry. Many studies have been conducted on the physical characteristics of different types of nanomaterials. Since their thermal conductivity may be abnormally increased with a less number of nanoparticles, nanofluids offer tremendous promise for enhancing heat transfer in fluids [1]. Equipping a porous medium, such as employing porous materials made of metal in channels and heat exchangers, is another way to improve heat transmission. Several researchers have looked at the methods of employing nanofluids and porous media. The efficiency of a conventional thermal system may be greatly improved by combining the use of porous media with nanofluids because they enhance the contact surface area between solid and liquid surfaces and improve effective thermal conductivity. The current analysis makes it clear that the majority of investigations are conducted using water-based nanofluids in cavities, whereas relatively small research is conducted with the porous media filled with nanofluids. Kuznetsov and Nield [2] examined the contact surface of the porous medium and used the analytical approach to evaluate the Soret effects and Brownian motion. The porous medium is used in the upright plates. Cheng and Minkowycz [3] looked at the age-old problem of natural convection.

The implications of viscous dissipation on nanofluid flow across an exponentially expanding surface have been discussed in previous studies [4,5]. When the Eckert number increases, a favorable effect is seen on the temperature profile. According to Mandal and Mukhopadhyay [6] in a micropolar fluid flow through a non-isothermal exponentially expanding sheet, the suction parameter has a negative effect on the velocity profile. Nanofluids are effective energy transfer fluids, and theoretical and experimental studies on these fluids highlight their vast applications and consequences, which include electronic cooling devices and heat exchangers. Hybrid nanofluids, which are favored over normal nanofluids due to their improved thermophysical characteristics, are the colloidal suspensions of base fluid containing two or more different nanoparticles. The synergistic effects enhance the thermal properties and prospective applications of nanofluid, which are advantageous in solar energy systems, hot rolling, thermal energy-producing systems, and nuclear system cooling (Hussien *et al.* [7]). In their investigation of the hybrid nanofluid flow across a stretching/shrinking sheet at the (magnetohydrodynamic [MHD]) hydromagnetic stagnation point, compared to the regular nanofluid, Junoh *et al.* [8] discovered that a hybrid nanofluid had a higher heat transfer rate. Following the micropolar fluid theory, Subhani and Nadeem [9] conducted comparative research on the normal and hybrid nanofluid flow caused by an exponentially extending surface. When a hybrid nanofluid was present, they sensed a greater temperature and a faster rate of heat transfer. Researchers [10–13] have taken into account a three-dimensional boundary-layer flow that is produced by the expansion of an incompressible ternary hybrid nanofluid over a rectangular closed domain in the x- and y-axes.

Gas-cooled nuclear reactors, gas turbines, nuclear power plants, spacecraft, and other high-heat activities all heavily rely on the phenomena of thermal radiation. Gireesha *et al.* [14] investigated the radiation behavior in three-dimensional MHD Jeffrey fluid flow *via* a stretched sheet in their article published in 2014, which revealed an increase in nanoparticle concentration and fluid temperature with changes in the radiation parameter. To investigate how thermophoresis and heat radiation affect a rotating, three-dimensional nanofluid flow that contains single-wall carbon nanotubes, Nasir *et al.* [15] used the homotopy method. They noted that the temperature of the nanofluid increases as the radiation parameter increases. Ramesh *et al.* [16], Gireesha *et al.* [17], and Besthapu *et al.* [18] investigated the Maxwell fluid flows and radiative Casson nanofluid resulting from a stretched surface, respectively. They found a considerable impact of radiation parameters on the rate of heat and mass transfer.

Natural convection, including heating effects, has been studied by Chen and Weng [19], while Davies *et al.* [20] investigated similar convection in horizontal microchannels with superhydrophobic inner surfaces. The direction of the microstructures causing superhydrophobicity was stressed in each of the two experiments. Temperature jumps and superhydrophobic slips were also taken into account. Another advancement is Ng and Wang [21], who considered isothermal and iso-flux heating modes for natural convection in a vertical slit microchannel. Jha and Gwandu [22] expanded on the work by taking into account electrically conducting fluid in the presence of a transverse magnetic field. In a rectangular, horizontal channel with varying viscosity, Bhatti and Zeeshan [23] examined the hydrodynamics and heat transmission of a fluid containing dust particles. Some of their key conclusions are as follows: (1) the effect of particle volume percentage causes the velocity profile to decline and (2) the relationship between the temperature profile and volume fraction is descending. The Eckert and Prandtl statistics show a reversal of the trend. Krishna and Chamkha [24] investigated the MHD squeezing flow of a water-based nanofluid through a porous medium between parallel disks. They considered the Hall current and solved the governing equations using the Galerkin optimal homotopy asymptotic method. In another study, Krishna *et al.* [25] examined heat and mass transfer in a micropolar fluid flow over an infinite vertical porous plate under an inclined magnetic field, employing a regular perturbation method. Additionally, Krishna *et al.* [26] focused on the Soret and Joule effects on MHD mixed convective flow past an infinite vertical porous plate, utilizing perturbation techniques to solve the equations. Krishna and Chamkha [27] investigated Hall and ion slip effects on MHD free convective rotating flow of nanofluids in a porous medium, with relevance to medical diagnostics. Moreover, Krishna *et al.* [28] analyzed the MHD flow of an electrically conducting second-grade fluid through a porous medium over a semi-infinite vertical stretching sheet, considering thermophoresis and thermal radiation. Further studies by Krishna *et al.* [25] and Krishna *et al.* [29] explored heat and mass transfer in micropolar fluid flow over vertical porous plates under inclined magnetic fields and the peristaltic MHD flow of Jeffrey fluids in porous media, respectively. They employed regular perturbation and exact solutions to understand the impacts of various parameters on flow behavior.

In this work, the MHD flow of an electrically conducting hybrid nanofluid is carried out while an alternative isothermal wall heating is provided to a vertical superhydrophobic microchannel. The capillarity pressure is judged to be within acceptable limits. As a result, the hybrid nanofluid may ascend the channel (buoyancy effects) without spilling onto the surface's tiny crevices. The presence of moisture and air are the two fundamental prerequisites for iron to rust. Even in mini- and microappliances devoid of water or other liquids, friction and other heat-producing processes result in the formation of steam, which wets the surfaces when it comes into contact. Because of this, engineers began to consider incorporating hydrophobic and even highly hydrophobic elements into their designs and production processes. To investigate the effects of the novel combination, this work seeks to impart a transverse magnetic field to the naturally convective flow of a hybrid nanofluid in a superhydrophobic microchannel. The results will enhance services in businesses that manufacture microchips, produce oil and gas, assemble small pieces of equipment, sterilize medical equipment, and other comparable businesses.

The following assumptions are considered in the given study:

1) The magnetic effect, nonlinear thermal buoyancy, heat source, thermal radiation, slip, and superhydrophobic conditions are considered.
2) Heat transfer rate and skin friction are analyzed in a hybrid nanofluid with **Case-1** TiO_2 + Ag and **Case-2** Cu + graphene, with the base fluid being H_2O.
3) Nanoparticles with uniform shapes are considered.
4) Regression statistics is applied to Nu and Cf data to study the significance of the parameter effect.

2 Problem formulation

Let us take a look at a fluid that conducts electricity that is constantly rising along a vertical channel formed by parallel heated plates. A particular microengineering process resulted in one of the surfaces being exceedingly difficult to wet (superhydrophobic). There was no tempering on the non-slip side.

According to Figure 1, the no-slip surface (NSS) is at $y = L$, while the superhydrophobic surface (SHS) is maintained at the position $y = 0$.

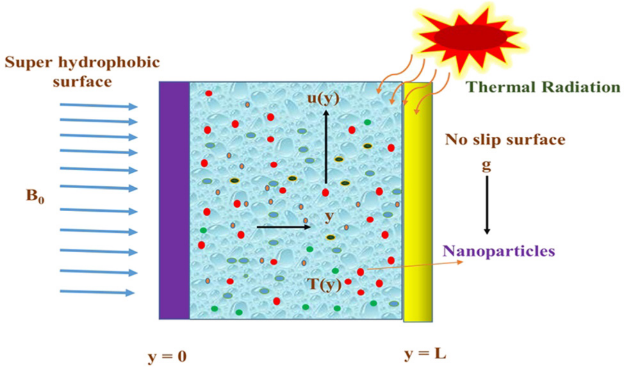

Figure 1: Physical model of the flow.

The Lorentz force of magnetism is characterized in the literature as the vector combination of the magnetic field vector $\vec{B}$ and the current density $\vec{J}$, *i.e.*, $\vec{F} = \vec{B} \times \vec{J}$.

Likewise, the current density is $\vec{J} = [\vec{V} \times \vec{B} + \vec{E}]\sigma_{\mathrm{hnf}}$, where σ_{hnf} is the hybrid nanofluid's electrical conductivity, $\vec{V}$ the velocity vector, and $\vec{E}$ the field of electricity. Combining both the aforementioned equations, we have $\vec{F} = [\vec{V} \times \vec{B} + \vec{E}]\sigma_{\mathrm{hnf}} \times \vec{B}$.

Taking one component from each of $\vec{B}$ and $\vec{V}$ while ignoring the electric field, *i.e.*, $\vec{B} = (0, B_0, 0)$, $\vec{E} = 0$, and $\vec{V} = (u, 0, 0)$, we have $\vec{F} = -\sigma_{\mathrm{hnf}}\vec{B}_0^2 u\hat{i}$.

Figure 1 depicts the directions of u and B_0.

Boundary conditions and the Boussinesq buoyancy approximation are used to create the system's governing equations. In the applied magnetic field and a porous media, an electrically conducting hybrid nanofluid was considered and a precise homotopy perturbation method (HPM) was used to solve the ordinary differential equation. Graphs were created in Maple software, and explanations were provided. As opposed to fluid or flow characteristics, a surface's superhydrophobicity is the main emphasis; hence, varied slip conditions and temperature jumps were employed for the different plates. This contrasts with the emphasis on gas rarefaction, which is inherent in the fluid's composition. Grooves, notches, holes, and cones are microengineered features that trap gases in their spaces and subsequently fill them. Until the capillary pressure is attained, the liquid is prevented from entering the empty gaps. Mixed boundary conditions are the outcome of the circumstance, which creates a hydrodynamic slip, and heat is carried far more slowly by gases than by liquids. The investigation was separated into two instances.

The dimensional resulting equations for the phenomenon discussed by Jha and Gwandu [22], Sajjan and Raju [30], and Zhang *et al.* [31] are as follows:

$$\frac{\mu_{\mathrm{hnf}}}{\rho_{\mathrm{hnf}}}\frac{\mathrm{d}^2u}{\mathrm{d}y^2} + (T - T_0)g(\beta_0)_{\mathrm{f}} + (T - T_0)^2g(\beta_1)_{\mathrm{f}} - \frac{\sigma_{\mathrm{hnf}}{B_0}^2u}{\rho_{\mathrm{hnf}}} - \frac{\mu_{\mathrm{hnf}}}{\rho_{\mathrm{hnf}}}\frac{u}{\kappa} = 0, \tag{1}$$

$$\frac{k_{\mathrm{hnf}}}{(\rho_{\mathrm{Cp}})_{\mathrm{hnf}}}\frac{\mathrm{d}^2T}{\mathrm{d}y^2} + \frac{\mu_{\mathrm{hnf}}}{(\rho_{\mathrm{Cp}})_{\mathrm{hnf}}}\left(\frac{\mathrm{d}u}{\mathrm{d}y}\right)^2 + \frac{\mu_{\mathrm{hnf}}}{(\rho_{\mathrm{Cp}})_{\mathrm{hnf}}}\frac{u^2}{\kappa} - \frac{1}{(\rho_{\mathrm{Cp}})_{\mathrm{hnf}}}\frac{\mathrm{d}q_{\mathrm{r}}}{\mathrm{d}y} + \frac{Q_0}{(\rho_{\mathrm{Cp}})_{\mathrm{hnf}}}(T - T_0) = 0. \tag{2}$$

Eq. (1) illustrates the impact of the Lorentz force on nonlinear buoyancy. Eq. (2) displays the thermal energy equation for the system in the presence of a sink and source, and the fluid's temperature between any two plates is $T = T(y)$.

Dimensional boundary constraints are provided by Jha and Gwandu [22], Sajjan and Raju [30], Zhang *et al.* [31]:

$$\left.\begin{aligned} T(y) &= (T_{\mathrm{w}} - T_0)B + T_0 \\ u(y) &= 0 \end{aligned}\right\} \text{at } y = L, \qquad \left.\begin{aligned} u(y) &= \left(\frac{\mathrm{d}u}{\mathrm{d}y}\right)\lambda' \\ T(y) &= (T_{\mathrm{w}} - T_0)A + T_0 + \gamma'\frac{\mathrm{d}T}{\mathrm{d}y} \end{aligned}\right\} \text{at } y = 0. \tag{3}$$

Type I: At $(B = 0, A = 1)$, SHS is heating.

Type II: At $(B = 1, A = 0)$, NSS is heating.

In Eq. (3), γ' and λ' are the temperature jump coefficients and the superhydrophobic velocity slip lengths, respectively.

The flow's characteristic velocity is given as follows:

$$U_0 = \frac{g(\beta_0)_{\mathrm{f}}L^2(T_{\mathrm{w}} - T_0)}{\nu_{\mathrm{f}}}. \tag{4}$$

Dimensionless equations and boundary conditions are given in Eqs. (5)–(7), which are enumerated as follows:

$$\frac{\left(\frac{\mu}{\rho}\right)_{\mathrm{hnf}}}{\left(\frac{\mu}{\rho}\right)_{\mathrm{f}}}\frac{\mathrm{d}^2U}{\mathrm{d}Y^2} + \theta + N\theta^2 - \frac{\left(\frac{\sigma}{\rho}\right)_{\mathrm{hnf}}}{\left(\frac{\sigma}{\rho}\right)_{\mathrm{f}}}M^2U - (\mathrm{Kp})^2\frac{\left(\frac{\mu}{\rho}\right)_{\mathrm{hnf}}}{\left(\frac{\mu}{\rho}\right)_{\mathrm{f}}}U = 0, \tag{5}$$

$$\frac{\left(\frac{k}{(\rho_{\mathrm{Cp}})}\right)_{\mathrm{hnf}}}{\left(\frac{k}{(\rho_{\mathrm{Cp}})}\right)_{\mathrm{f}}}\left[\frac{\mathrm{d}^2\theta}{\mathrm{d}Y^2}\right] + \frac{\left(\frac{\mu}{(\rho_{\mathrm{Cp}})}\right)_{\mathrm{hnf}}}{\left(\frac{\mu}{(\rho_{\mathrm{Cp}})}\right)_{\mathrm{f}}}\mathrm{Ec}\,\mathrm{Pr}\left[\left(\frac{\mathrm{d}U}{\mathrm{d}Y}\right)^2 + U^2(Kp)^2\right] + \frac{(\rho_{\mathrm{Cp}})_{\mathrm{f}}}{(\rho_{\mathrm{Cp}})_{\mathrm{hnf}}}\frac{4R}{3}\frac{\mathrm{d}^2\theta}{\mathrm{d}Y^2} + \frac{(\rho_{\mathrm{Cp}})_{\mathrm{f}}}{(\rho_{\mathrm{Cp}})_{\mathrm{hnf}}}Q_T\theta = 0, \tag{6}$$

$$\left.\begin{aligned} \theta(Y) &= B \\ U(Y) &= 0 \end{aligned}\right\} \text{at } y = 1, \qquad \left.\begin{aligned} U(Y) &= \left(\frac{\mathrm{d}U}{\mathrm{d}Y}\right)\lambda \\ \theta(Y) &= A + \gamma\left(\frac{\mathrm{d}\theta}{\mathrm{d}Y}\right) \end{aligned}\right\} \text{at } y = 0. \tag{7}$$

The following equation provides the skin friction at two different surfaces:

$$\tau_0 = \frac{\mu_{\mathrm{hnf}}}{\mu_{\mathrm{f}}}\frac{\mathrm{d}U}{\mathrm{d}Y}\bigg|_{Y=0} \Rightarrow \mathrm{Re}^{\frac{1}{2}}\tau_0 = \frac{U'(0)}{z_1},$$
$$\tau_1 = \frac{\mu_{\mathrm{hnf}}}{\mu_{\mathrm{f}}}\frac{\mathrm{d}U}{\mathrm{d}Y}\bigg|_{Y=1} \Rightarrow \mathrm{Re}^{\frac{1}{2}}\tau_1 = \frac{U'(1)}{z_1}. \tag{8}$$

The expressions for the mass flow rate and bulk temperature provided by Jha and Gwandu [22], Sajjan and Raju [30], and Zhang *et al.* [31] are as follows:

$$Q = \int_0^1 U(Y)\mathrm{d}Y; \quad \theta_{\mathrm{b}} = \frac{\left(\int_0^1 U(Y)\theta(Y)\mathrm{d}Y\right)}{Q}. \tag{9}$$

The equation that represents the rate of heat transfer, expressed as Nusselt numbers, is as follows:

$$\mathrm{Nu}_0 = \frac{1}{\theta_{\mathrm{b}}}\left[\frac{L^2\left(-k_{\mathrm{hnf}}\frac{\mathrm{d}\theta}{\mathrm{d}Y} + q_{\mathrm{r}}\right)}{k_{\mathrm{f}}(T_{\mathrm{w}} - T_0)}\right]\Bigg|_{Y=0}$$
$$\Rightarrow \mathrm{Re}^{-\frac{1}{2}}\ \mathrm{Nu}_0 = \frac{-\left(z_5 + \frac{4R}{3}\right)\theta'(0)}{\theta_{\mathrm{b}}},$$
$$\mathrm{Nu}_1 = \frac{1}{\theta_{\mathrm{b}}}\left[\frac{L^2\left(k_{\mathrm{hnf}}\frac{\mathrm{d}\theta}{\mathrm{d}Y} + q_{\mathrm{r}}\right)}{k_{\mathrm{f}}(T_{\mathrm{w}} - T_0)}\right]\Bigg|_{Y=1}$$
$$\Rightarrow \mathrm{Re}^{-\frac{1}{2}}\ \mathrm{Nu}_1 = \frac{\left(z_5 - \frac{4R}{3}\right)\theta'(1)}{\theta_{\mathrm{b}}}. \tag{10}$$

The efficient thermophysical models of the hybrid nanofluid are provided by

Here, we considered $\phi_1 = 0.02$ and $\phi_2 = 0.05$

The following may be deduced from Eqs. (5) and (6) given the similarity variables and efficient thermophysical model described earlier:

$$\frac{1}{z_1 z_2}\frac{\mathrm{d}^2U}{\mathrm{d}Y^2} + \theta + N\theta^2 - \frac{z_3}{z_2}M^2U - (\mathrm{Kp})^2\frac{1}{z_1 z_2}U = 0, \tag{11}$$

$$\frac{z_5}{z_4}\left[\frac{\mathrm{d}^2\theta}{\mathrm{d}Y^2}\right] + \frac{1}{z_1 z_2}\mathrm{Ec}\ \mathrm{Pr}\left[\left(\frac{\mathrm{d}U}{\mathrm{d}Y}\right)^2 + U^2(\mathrm{Kp})^2\right] + \frac{4R}{3z_4}\frac{\mathrm{d}^2\theta}{\mathrm{d}Y^2} + \frac{Q_{\mathrm{T}}\theta}{z_4} = 0. \tag{12}$$

3 Methodology

The technique of HPM: the following equation is used to illustrate the key concept of this approach:

$$C(v) - f(r) = 0 \quad r \in \Omega. \tag{13}$$

Taking the boundary conditions into account:

$$D\left(v, \frac{\partial v}{\partial n}\right) = 0 \quad r \in \Gamma. \tag{14}$$

In this scenario, Γ denotes the edge of the Ω domain, C is a generic differential operator, D is a boundary operator, and $f(r)$ is a well-known analytical function.

The linear and nonlinear components of C may be separated into L and N, where L and N stand for the linear and nonlinear components, respectively. Eq. (13) can thus be rewritten as follows:

$$N(v) + L(v) - f(r) = 0 \quad r \in \Omega. \tag{15}$$

The following equation illustrates the structure of homotopy perturbation:

Dynamic viscosity:	$\frac{\mu_{\mathrm{hnf}}}{\mu_{\mathrm{f}}} = [(1 - \phi_2)^{-2.5}(1 - \phi_1)^{-2.5}] = \frac{1}{z_1}.$
Density:	$\frac{\rho_{\mathrm{hnf}}}{\rho_{\mathrm{f}}} = \phi_2\left(\frac{\rho_{\mathrm{s2}}}{\rho_{\mathrm{f}}}\right) + (1 - \phi_2)\left[\phi_1\left(\frac{\rho_{\mathrm{s1}}}{\rho_{\mathrm{f}}}\right) + 1 - \phi_1\right] = z_2.$
Electrical conductivity:	$\frac{\sigma_{\mathrm{hnf}}}{\sigma_{\mathrm{f}}} = 1 + \frac{3\left(\frac{\phi_2\sigma_2 + \phi_1\sigma_1}{\sigma_{\mathrm{f}}} - (\phi_2 + \phi_1)\right)}{2 - \left(\frac{\phi_1\sigma_1 + \phi_2\sigma_2}{\sigma_{\mathrm{f}}} - (\phi_1 + \phi_2)\right) + \left(\frac{\phi_1\sigma_1 + \phi_2\sigma_2}{(\phi_1 + \phi_2)\sigma_{\mathrm{f}}}\right)} = z_3.$
Specific heat:	$\frac{(\rho C_{\mathrm{p}})_{\mathrm{hnf}}}{(\rho C_p)_{\mathrm{f}}} = \phi_2\left(\frac{(\rho C_{\mathrm{p}})_{\mathrm{s2}}}{(\rho C_{\mathrm{p}})_{\mathrm{f}}}\right) + (1 - \phi_2)\left[1 - \phi_1 + \phi_1\left(\frac{(\rho C_{\mathrm{p}})_{\mathrm{s1}}}{(\rho C_{\mathrm{p}})_{\mathrm{f}}}\right)\right] = z_4.$
Thermal conductivity:	$z_5 = \frac{k_{\mathrm{hnf}}}{k_{\mathrm{f}}} = \left(\left(\frac{k_{\mathrm{hnf}}}{k_{\mathrm{nf}}}\right)\left(\frac{k_{\mathrm{nf}}}{k_f}\right)\right)$ where $\frac{k_{\mathrm{hnf}}}{k_{\mathrm{nf}}} = \frac{2k_{\mathrm{nf}} - 2\phi_2(k_{\mathrm{nf}} - k_{s2}) + k_{s2}}{2k_{\mathrm{nf}} + 2\phi_2(k_{\mathrm{nf}} - k_{s2}) + k_{s2}}$ and $k_{\mathrm{nf}} = \left(\frac{2k_{\mathrm{f}} + k_{s1} - 2\phi_1(k_f - k_{s1})}{2k_{\mathrm{f}} + k_{s1} + 2\phi_1(k_f - k_{s1})}\right)k_f$

$$H(w,p) = (1-p)[L(w) - L(v_0)] + p[C(w) - f(r)] = 0, \tag{16}$$

where

$$v(r,p) : \Omega \times [0,1] \to R. \tag{17}$$

The initial approximation that meets the boundary condition is called u_0, and the embedding parameter $p \in [0,1]$ is used. As a power series in p, the solution to Eq. (16) may be defined as follows:

$$w = w_0 + pw_1 + p^2 w_2 + \ldots \tag{18}$$

The following is the best approximation for the solution:

$$v = \lim_{p \to 1} w = w_0 + w_1 + w_2 + \ldots \tag{19}$$

HPM solution for the governing Eqs. (11) and (12):

$$\begin{gathered} p^0 : \frac{U_0''}{z_1 z_2} = 0, \quad \left(\frac{z_5}{z_4} + \frac{4R}{3z_4}\right)\theta''_0 = 0, \\ \theta_0(0) = A + \gamma\, \theta_0'(0), \quad U_0(0) = \lambda\, U_0'(0), \; U_0(1) = 0, \\ \theta_0(1) = B, \end{gathered} \tag{22}$$

$$\begin{gathered} p^1 : \frac{U_1''}{z_1 z_2} + \theta_0 + N{\theta_0}^2 - \frac{z_3 (M)^2 U_0}{z_2} - \frac{(\mathrm{Kp})^2 U_0}{z_1 z_2} = 0, \\ \left(\frac{z_5}{z_4} + \frac{4R}{3z_4}\right)\theta''_1 + \frac{\Pr \mathrm{Ec}\,((U_0')^2 + (U_0)^2 (\mathrm{Kp})^2)}{z_1 z_2} + \frac{Q_{\mathrm{T}} \theta_0}{z_4} \\ = 0, \\ U_1(0) = \lambda\, U_1'(0), \; \theta_1(0) = 0, \; U_1(1) = 0, \; \theta_1(1) = 0, \end{gathered} \tag{23}$$

$$\begin{gathered} p^2 : \frac{U_2''}{z_1 z_2} + \theta_1 + 2N\theta_0\theta_1 - \frac{z_3 (M)^2 U_1}{z_2} - \frac{(\mathrm{Kp})^2 U_1}{z_1 z_2} = 0, \\ \left(\frac{z_5}{z_4} + \frac{4R}{3z_4}\right)\theta''_2 + \frac{\Pr \mathrm{Ec}\,(2U_0' U_1' + 2U_0 U_1 (\mathrm{Kp})^2)}{z_1 z_2} + \frac{Q_T \theta_1}{z_4} \\ = 0, \\ U_2(0) = \lambda\, U_2'(0), \; \theta_2(0) = 0, \; U_2(1) = 0, \; \theta_2(1) = 0. \end{gathered} \tag{24}$$

$$\left.\begin{aligned} &\frac{(1-p)(U_0'' + pU_1'' + p^2 U_2'')}{z_1 z_2} + p\left(\begin{aligned} &\frac{U_0'' + pU'' + p^2 U_2''}{z_1 z_2} + \theta_0 + p\,\theta_1 + p^2\theta_2 + N\,(\theta_0 + p\,\theta_1 + p^2\theta_2)^2 \\ &- \frac{z_3 M^2 (U_0 + p\,U_1 + p^2 U_2)}{z_2} - \frac{(\mathrm{Kp})^2 (U_0 + p\,U_1 + p^2 U_2)}{z_1 z_2} \end{aligned}\right) = 0, \\ &(1-p)(\theta_0'' + p\theta_1'' + p^2\theta_2'')\left(\frac{z_5}{z_4} + \frac{4R}{3z_4}\right) + p\left(\begin{aligned} &\left(\frac{z_5}{z_4} + \frac{4R}{3z_4}\right)(\theta_0'' + p\theta_1'' + p^2\theta_2'') + \frac{Q_T(\theta_0 + p\theta_1 + p^2\theta_2)}{z_4} + \\ &\frac{\Pr \mathrm{Ec}\,((U_0' + pU_1' + p^2 U_2')^2 + (U_0 + p\,U_1 + p^2 U_2)^2 (\mathrm{Kp})^2)}{z_1 z_2} \end{aligned}\right) = 0. \end{aligned}\right\} \tag{20}$$

Assuming that the solution can be expressed as a series in terms of the embedding parameter p, we consider U and θ as follows:

$$U = U_0 + p\,U_1 + p^2 U_2 + \ldots, \quad \theta = \theta_0 + p\,\theta_1 + p^2\theta_2 + \ldots. \tag{21}$$

Substitute the series expansions into the homotopy equations, and equate the coefficients of like powers of p. This generates a series of linear differential equations that can be solved sequentially.

Assuming $U_0'' = \theta_0'' = 0$, inserting U and θ from Eq. (21) into Eq. (20), and then simplifying and rearranging based on the powers of p-terms, we obtain the following results:

Solving Eqs. (22)–(24) with boundary conditions, we have

$$U_0 = 0, \; \theta_0 = -\frac{Y(A-B)}{\gamma + 1} + \frac{A + B\gamma}{\gamma + 1}, \tag{25}$$

By following these steps, HPM provides a systematic approach to solving the given system of nonlinear differential equations analytically, resulting in an approximate series solution that satisfies the boundary conditions and converges to the true solution.

$$\begin{aligned} U_1 &= -\frac{1}{(\gamma+1)^2}\left(z_1z_2\left(\begin{matrix}\dfrac{(A-B)(AN-BN)Y^4}{12} + \dfrac{((-B\gamma-A)+(-\gamma-1-N(A+B\gamma))(A-B))Y^3}{6}\\ +\dfrac{(-B\gamma-A)(-N(A+B\gamma)-\gamma-1)Y^2}{2}\end{matrix}\right)\right)\\ &+\frac{1}{12(\gamma^2\lambda+\gamma^2+2\gamma\lambda+2\gamma+\lambda+1)}\left(z_1z_2\left(\begin{matrix}6B^2\gamma^2N+8ABN\gamma+4B^2\gamma N+3A^2N+2ABN+B^2N+\\ 6B\gamma^2+4A\gamma+8B\gamma+4A+2B\end{matrix}\right)Y\right)\\ &+\frac{1}{12(\gamma^2\lambda+\gamma^2+2\,\gamma\,\lambda+2\,\gamma+\lambda+1)}\left(\lambda\, z_1z_2\left(\begin{matrix}6B^2\gamma^2N+8ABN\gamma+4B^2\gamma N+3A^2N+2ABN+B^2N+\\ 6B\gamma^2+4A\gamma+8B\gamma+4A+2B\end{matrix}\right)\right), \end{aligned} \tag{26}$$

$$\theta_1 = \frac{1}{2(\gamma+1)(3z_5+4R)}\left(Q_T(AY^3-BY^3-3\gamma BY^2-3AY^2)+\frac{Q_T(3\gamma B+2A+B)Y(\gamma+1)(3z_5+4R)}{4R\gamma+3z_5\gamma+4R+3z_5}\right),$$

$$\theta_2 = \frac{1}{40(\gamma+1)(3z_5+4R)^2}\left(\begin{matrix}{Q_T}^2(3(A-B)Y^5+5(-3\gamma B-3A)Y^4+10(3\gamma B+2A+B)Y^3)\\ \dfrac{{Q_T}^2(15\gamma B+8A+7B)Y(\gamma+1)(3z_5+4R)^2}{16R^2\gamma+24Rz_5\gamma+9{z_5}^2(\gamma+1)+16R^2+24z_5R}\end{matrix}\right). \tag{27}$$

After substituting, the following parameter values $\mathrm{Pr} = 6.8$, $\mathrm{Kp} = 1$, $M = 1$, $N = 1$, $\mathrm{Ec} = 1$, $\lambda = 0.5$, $\gamma = 0.5$, $R = 1$, and $Q_T = 1$ in Eqs. (25)–(27),

when superhydrophobic heating surface is heated ($B = 0, A = 1$), and

for HNF-1(a mixture of TiO_2 and silver Ag),

$$U_0 = 0, \quad \theta_0 = -\frac{2Y}{3} + \frac{2}{3}, \tag{28}$$

$$\begin{aligned} U_1 &= -\frac{11{,}954}{250{,}843}Y^4 + \frac{29{,}353}{87{,}992}Y^3 - \frac{15{,}584}{21{,}801}Y^2\\ &+ \frac{25{,}723}{89{,}962}Y + \frac{15{,}584}{109{,}005}, \\ \theta_1 &= \frac{6{,}410}{150{,}887}Y^3 - \frac{7{,}313}{57{,}381}Y^2 + \frac{13{,}723}{161{,}515}Y, \end{aligned} \tag{29}$$

$$\begin{aligned} U_2 &= -\frac{1{,}057}{1{,}342{,}042}Y^6 + \frac{3{,}673}{223{,}024}Y^5 - \frac{15{,}719}{205{,}196}Y^4\\ &+ \frac{3{,}973}{73{,}580}Y^3 + \frac{9{,}679}{66{,}860}Y^2 - \frac{6{,}589}{71{,}704}Y\\ &- \frac{6{,}589}{143{,}408}, \\ \theta_2 &= -\frac{627}{772{,}045}Y^5 + \frac{627}{154{,}409}Y^4 - \frac{836}{154{,}409}Y^3\\ &+ \frac{1672}{772{,}045}Y. \end{aligned} \tag{30}$$

For HNF-2 (a mixture of copper and graphene)

$$U_0 = 0, \quad \theta_0 = -\frac{2Y}{3} + \frac{2}{3} \tag{31}$$

$$\begin{aligned} U_1 &= -\frac{6{,}199}{165{,}186}Y^4 + \frac{6{,}199}{23{,}598}Y^3 - \frac{28{,}512}{50{,}651}Y^2\\ &+ \frac{6{,}199}{27{,}531}Y + \frac{6{,}199}{55{,}062}, \\ \theta_1 &= \frac{15{,}321}{362{,}639}Y^3 - \frac{48{,}395}{381{,}827}Y^2 + \frac{14{,}713}{174{,}124}Y, \end{aligned} \tag{32}$$

$$\begin{aligned} U_2 &= -\frac{767}{1{,}216{,}041}Y^6 + \frac{4{,}769}{365{,}611}Y^5 - \frac{7{,}532}{124{,}465}Y^4\\ &+ \frac{4{,}721}{110{,}551}Y^3 + \frac{7{,}965}{69{,}869}Y^2 - \frac{22{,}118}{305{,}493}Y\\ &- \frac{11{,}059}{305{,}493}, \\ \theta_2 &= -\frac{789}{982{,}289}Y^5 + \frac{1{,}726}{429{,}767}Y^4 - \frac{6{,}904}{1{,}289{,}301}Y^3\\ &+ \frac{1{,}463}{683{,}027}Y. \end{aligned} \tag{33}$$

When NSS is heated ($B = 1, A = 0$) and
for HNF-1 (a mixture of TiO_2 and Ag),

$$U_0 = 0, \quad \theta_0 = \frac{2Y}{3} + \frac{1}{3}, \tag{34}$$

$$\begin{aligned} U_1 &= -\frac{11{,}954}{250{,}843}Y^4 - \frac{15{,}584}{65{,}403}Y^3 - \frac{25{,}723}{89{,}962}Y^2\\ &+ \frac{22{,}093}{57{,}950}Y + \frac{25{,}723}{134{,}943}, \\ \theta_1 &= -\frac{6{,}410}{150{,}887}Y^3 - \frac{7{,}313}{114{,}762}Y^2 + \frac{9{,}119}{85{,}862}Y, \end{aligned} \tag{35}$$

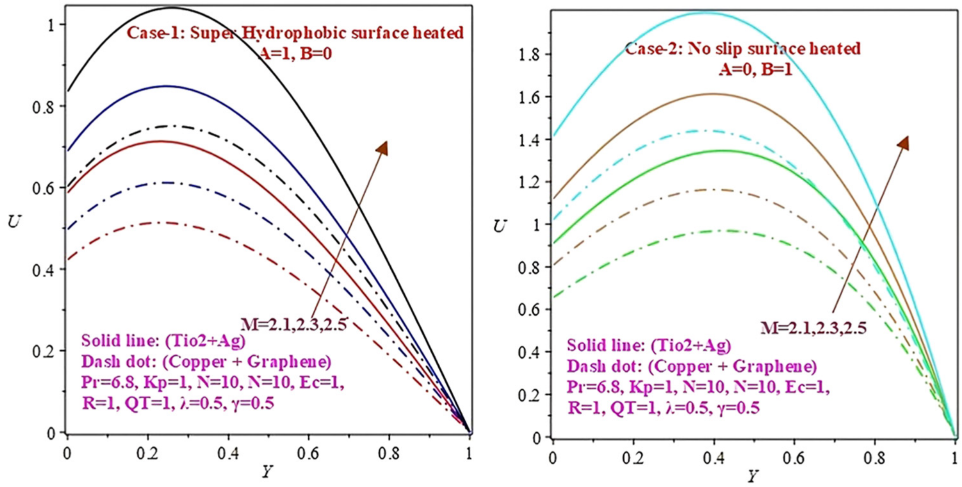

Figure 2: Effects of the magnetic parameter on the velocity of two hybrid nanoparticles when the NSS and SHS are heated.

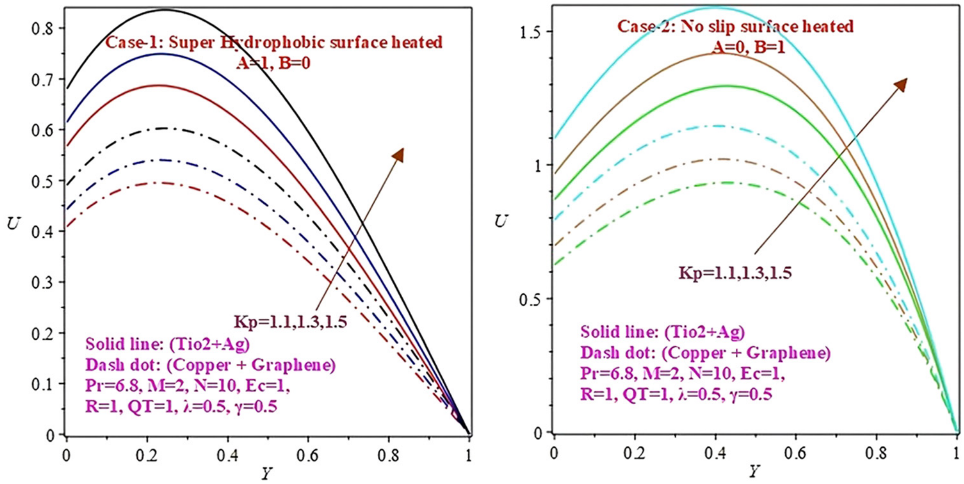

Figure 3: Effects of the porosity parameter on the velocity of two hybrid nanoparticles when the NSS and SHS are heated.

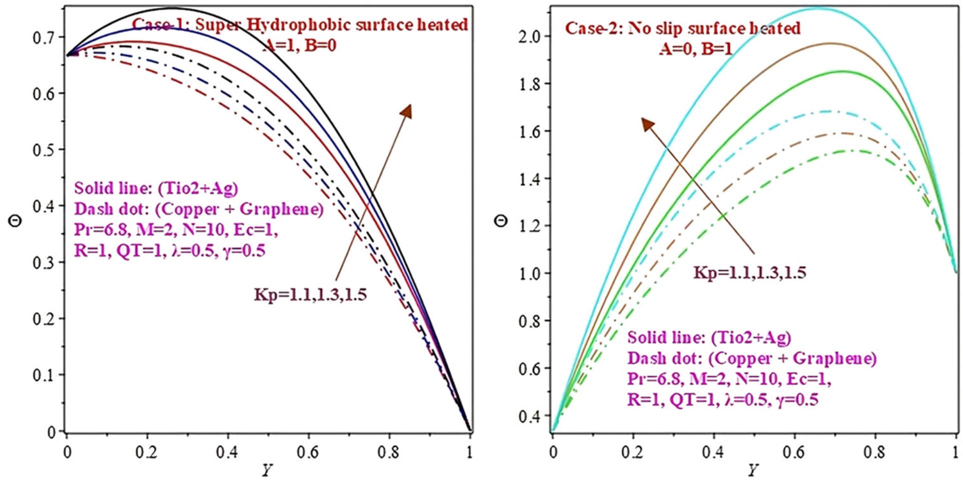

Figure 4: Effects of the porosity parameter for two hybrid nanoparticles on the temperature when the NSS and SHS are heated.

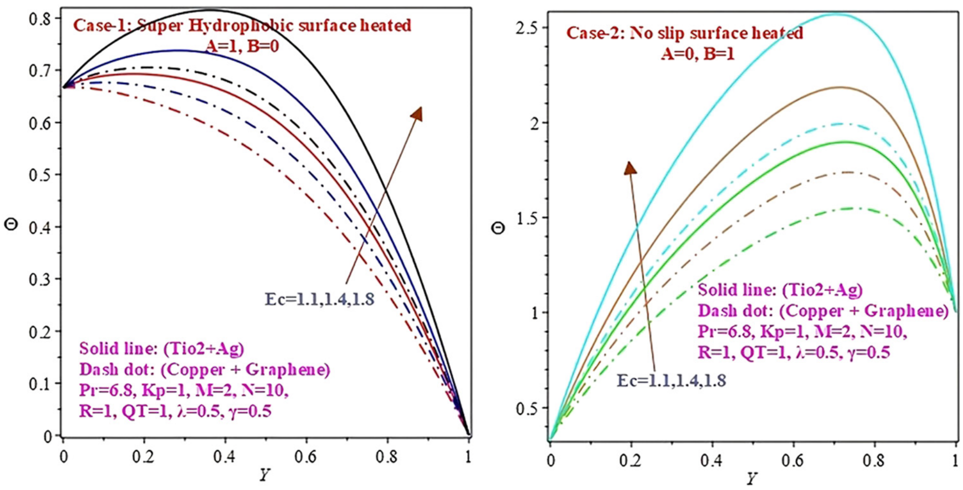

Figure 5: Effects of the Eckert number for two hybrid nanoparticles on the temperature when the NSS and SHS are heated.

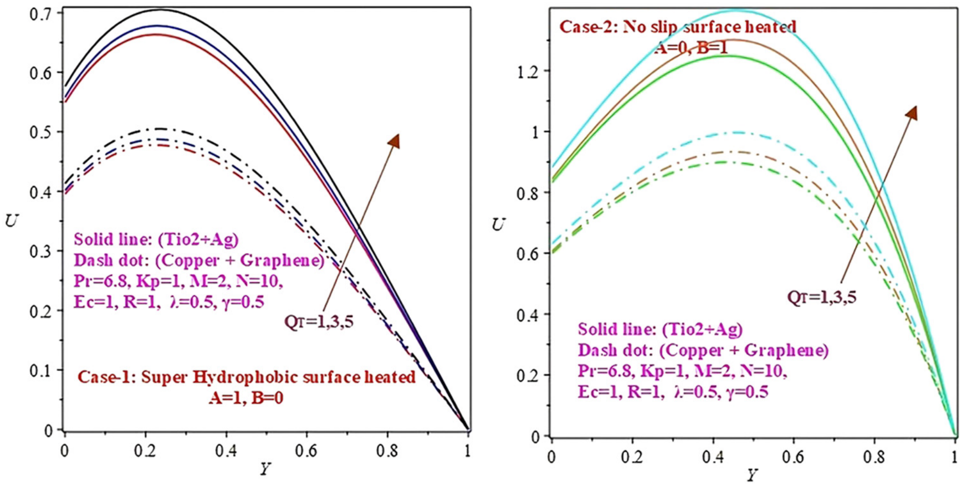

Figure 6: Effects of Q_T for two hybrid nanoparticles on the velocity when the NSS and SHS are heated.

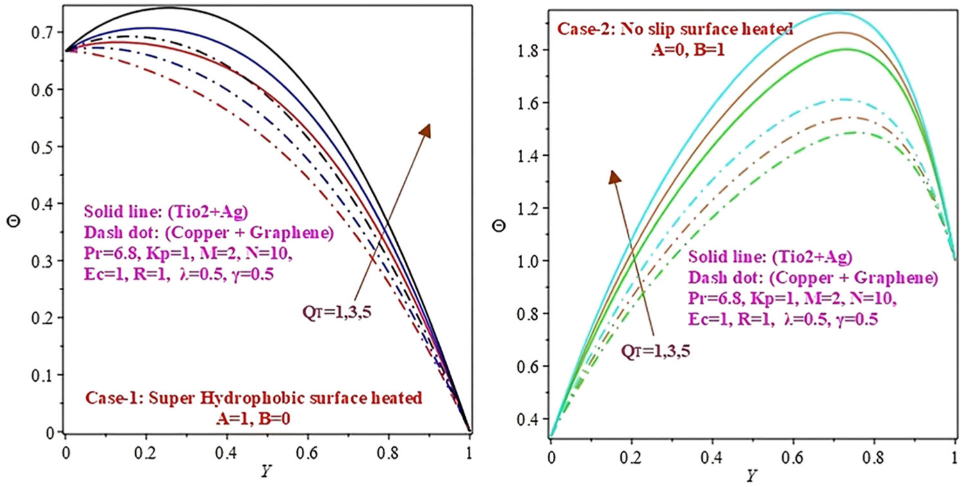

Figure 7: Effects of Q_T for two hybrid nanoparticles on the temperature when the NSS and SHS are heated.

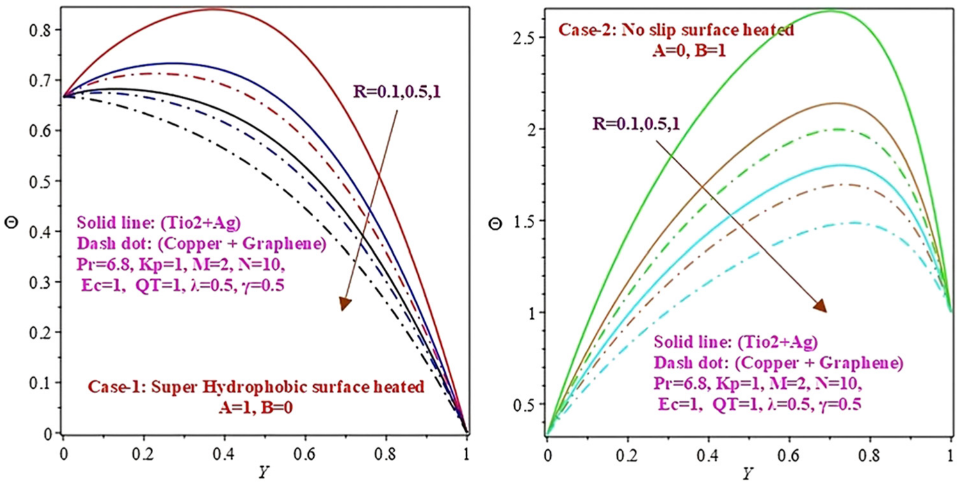

Figure 8: Effects of thermal radiation for two hybrid nanoparticles on the temperature when the NSS and SHS are heated.

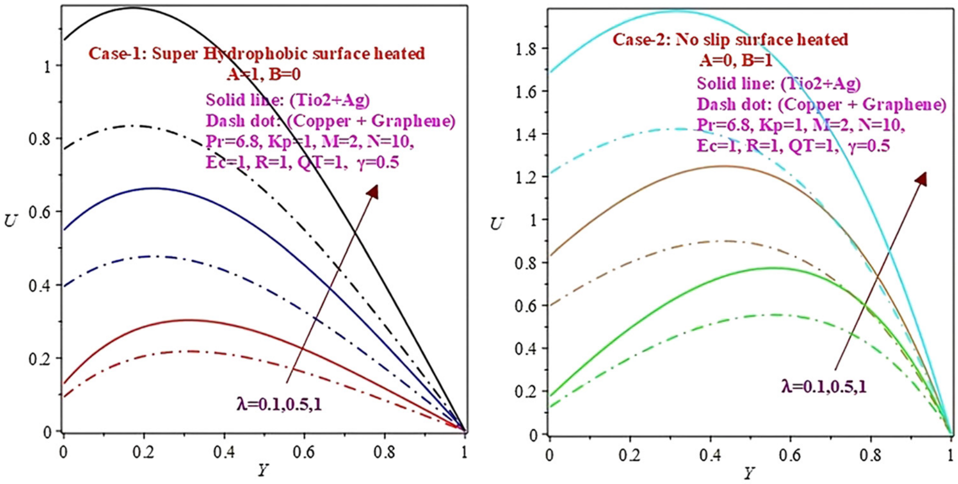

Figure 9: Effects of the slip length on the velocity for two hybrid nanoparticles when the NSS and SHS are heated.

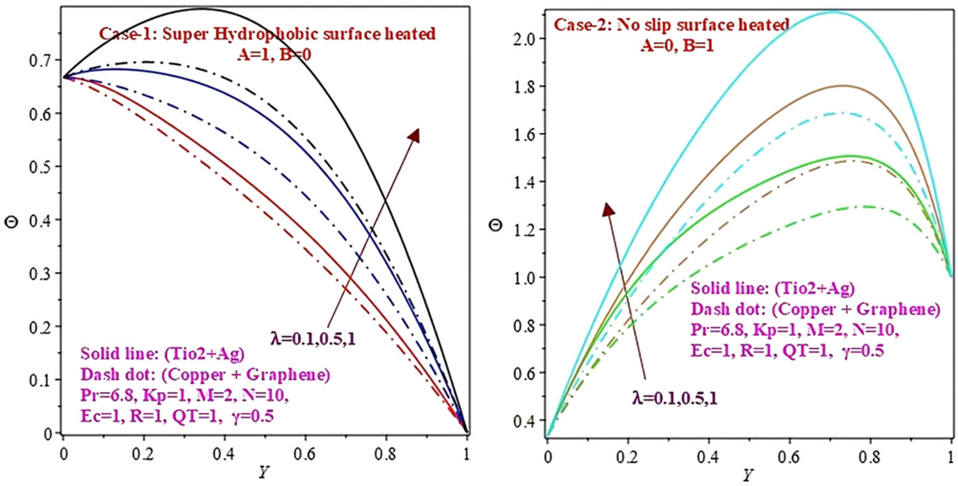

Figure 10: Effects of the slip length on the temperature for two hybrid nanoparticles when the NSS and SHS are heated.

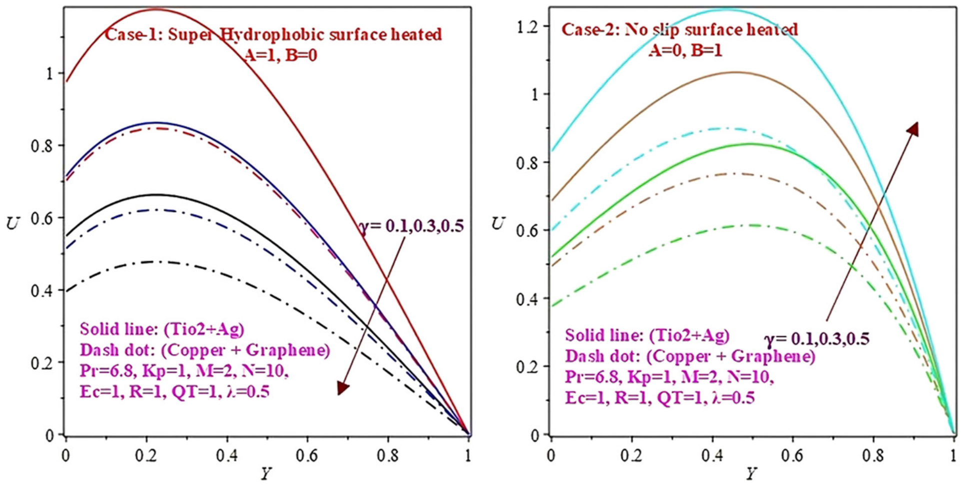

Figure 11: Effects of the temperature jump coefficient on the velocity for two hybrid nanoparticles when the NSS and SHS are heated.

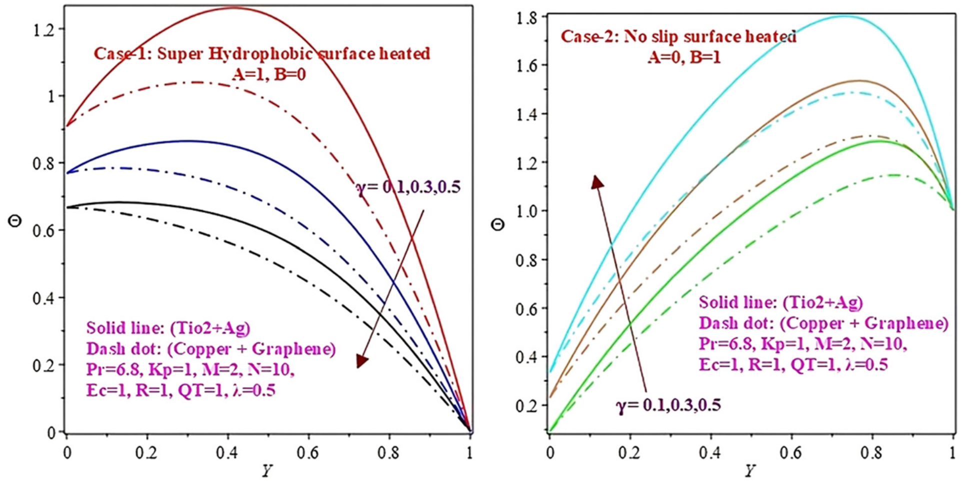

Figure 12: Effects of the temperature jump coefficient on the temperature for two hybrid nanoparticles when the NSS and SHS are heated.

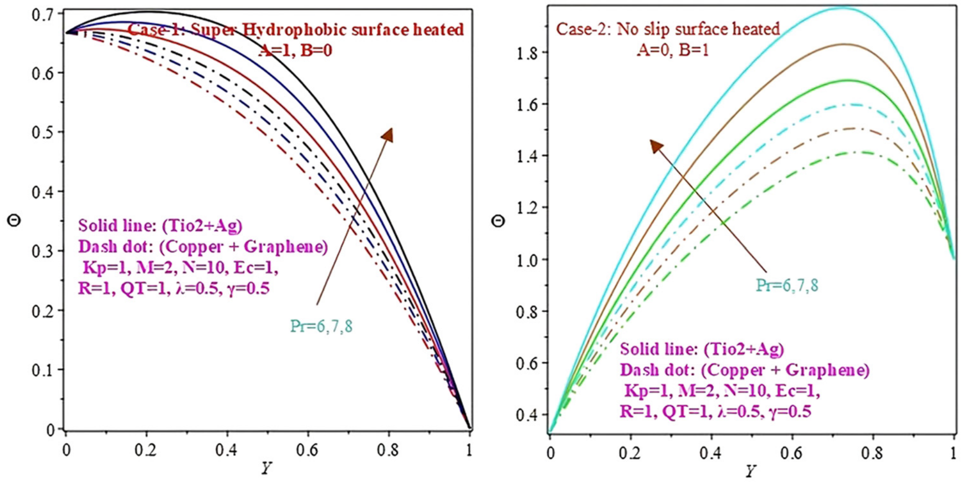

Figure 13: Effects of Prandtl number Pr for two hybrid nanoparticles on the temperature when the NSS and SHS are heated.

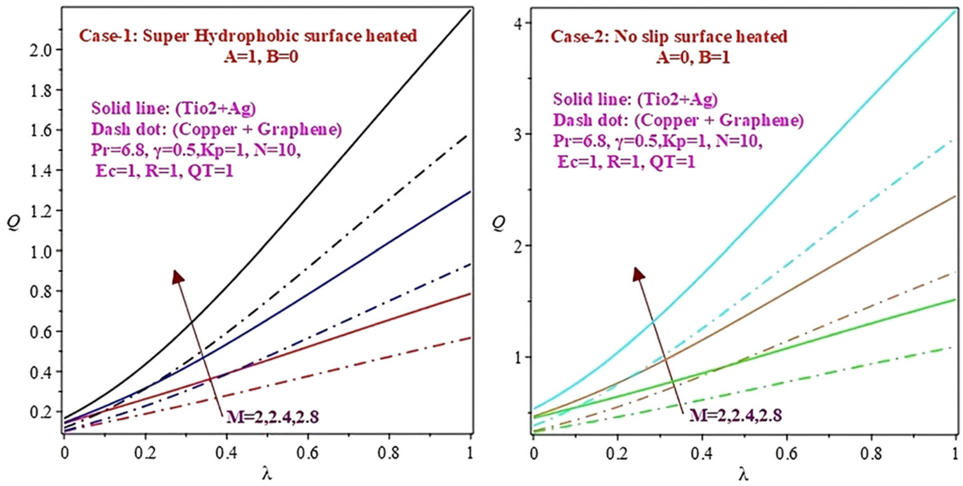

Figure 14: Effects of the magnetic parameter for two hybrid nanoparticles on the flow rate when the NSS and SHS are heated.

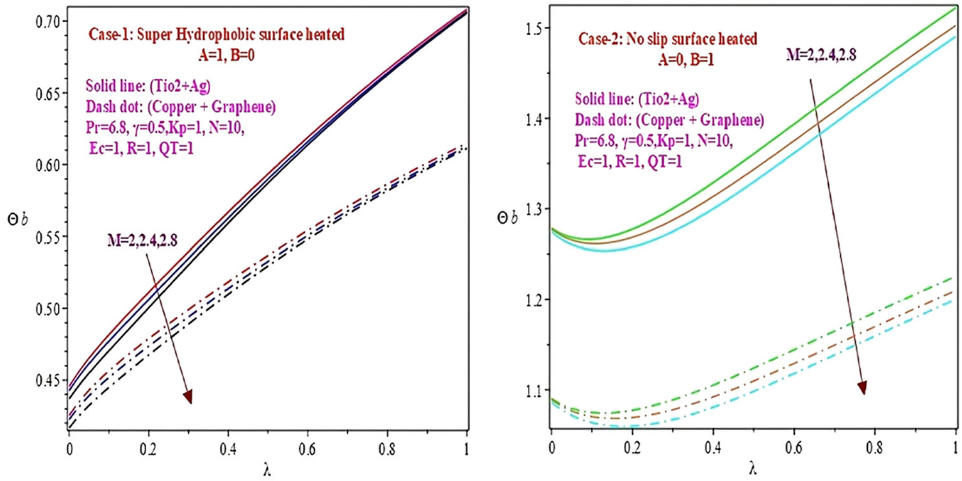

Figure 15: Effects of the magnetic parameter for two hybrid nanoparticles on the bulk temperature when the NSS and SHS are heated.

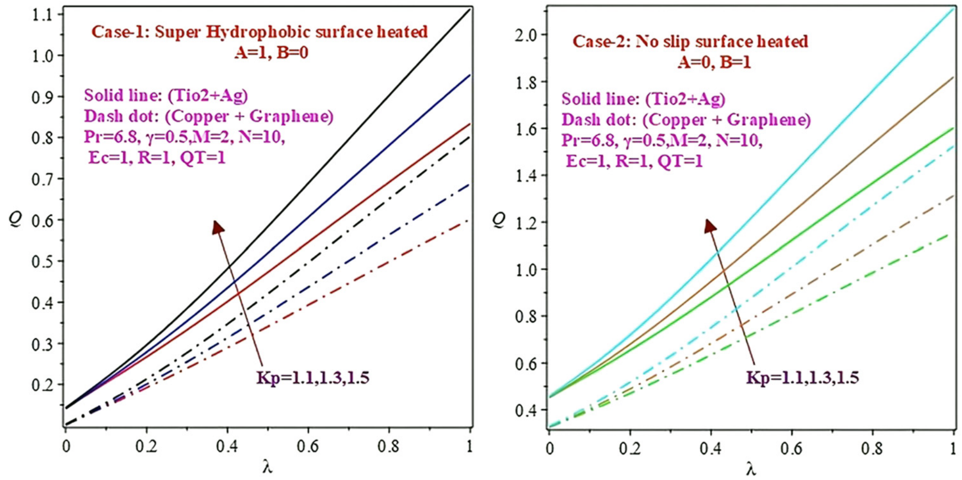

Figure 16: Effects of the porosity parameter for two hybrid nanoparticles on the flow rate when the NSS and SHS are heated.

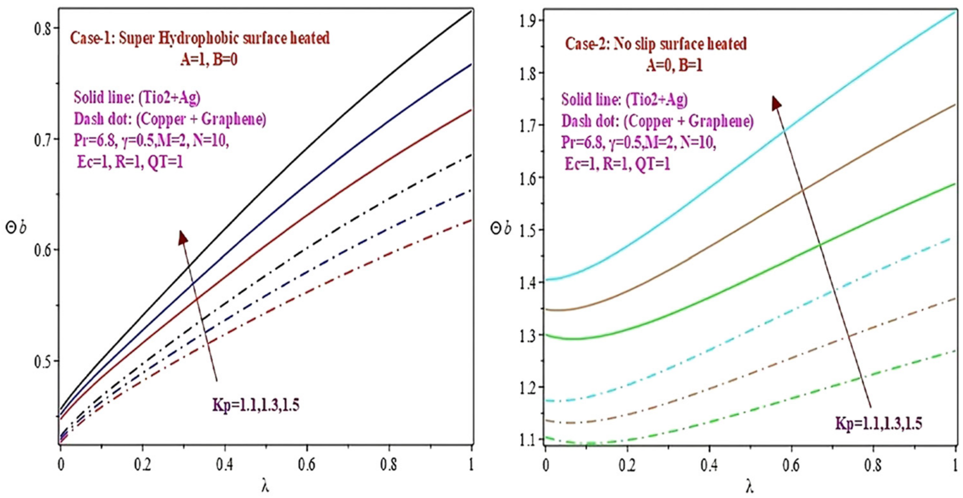

Figure 17: Effects of the porosity parameter for two hybrid nanoparticles on the bulk temperature when the NSS and SHS are heated.

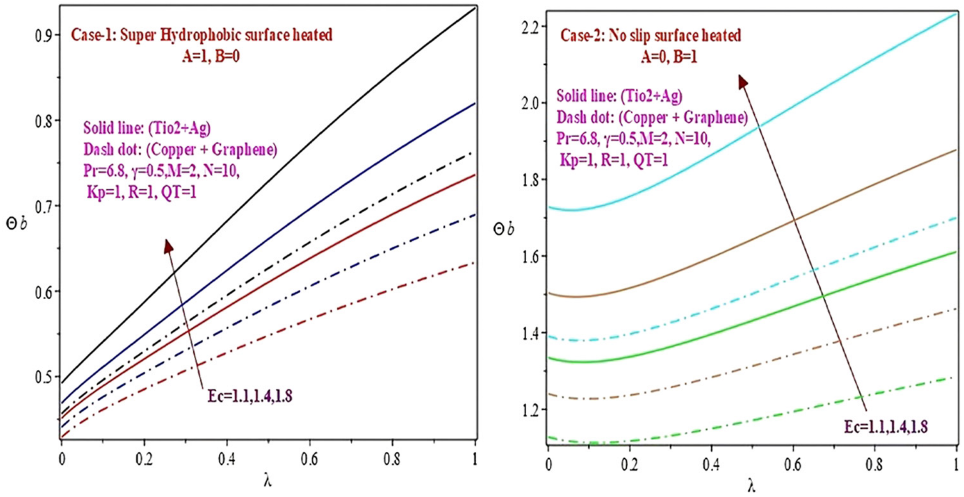

Figure 18: Effects of Eckert number for two hybrid nanoparticles on the bulk temperature when the NSS and SHS are heated.

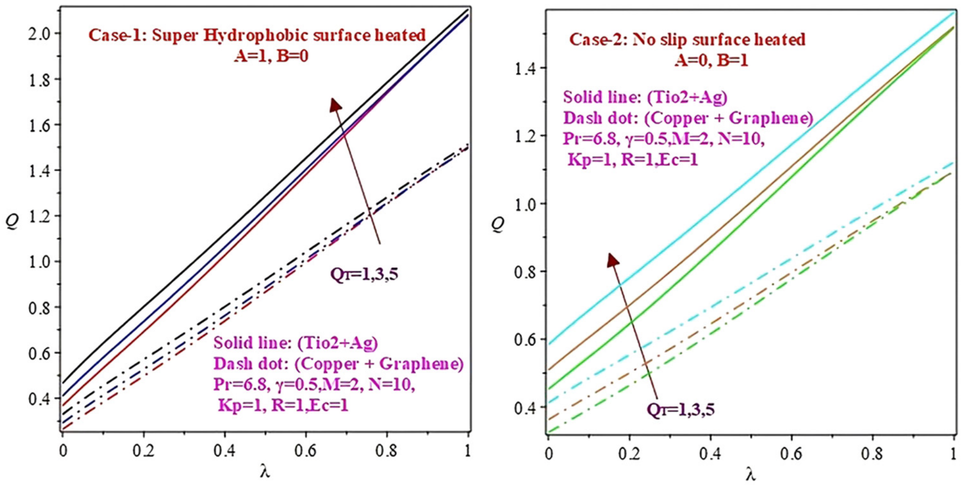

Figure 19: Effects of Q_T for two hybrid nanoparticles on the flow rate when the NSS and SHS are heated.

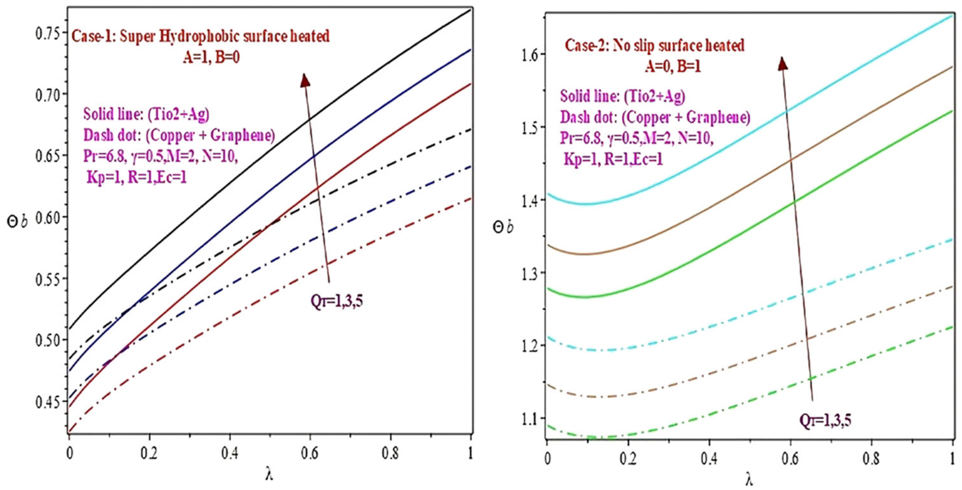

Figure 20: Effects of Q_T for two hybrid nanoparticles on the bulk temperature when the NSS and SHS are heated.

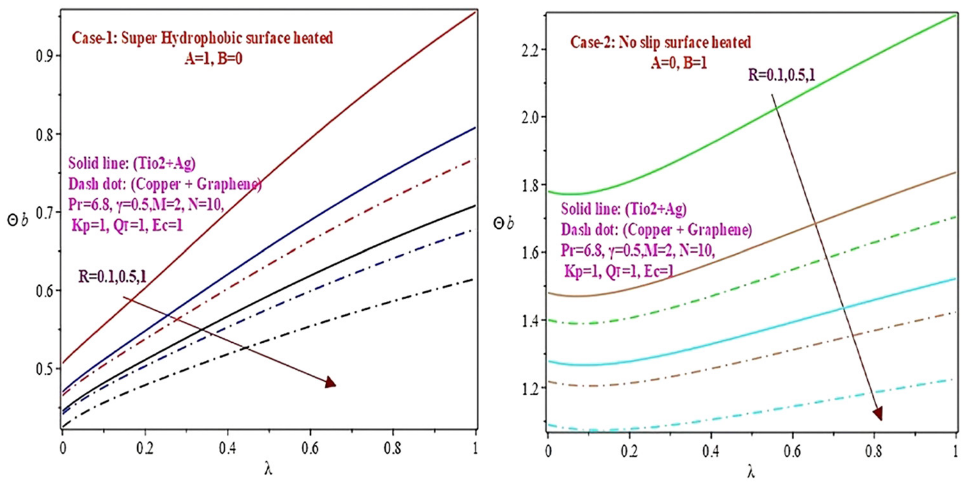

Figure 21: Effects of thermal radiation for two hybrid nanoparticles on the bulk temperature when the NSS and SHS are heated.

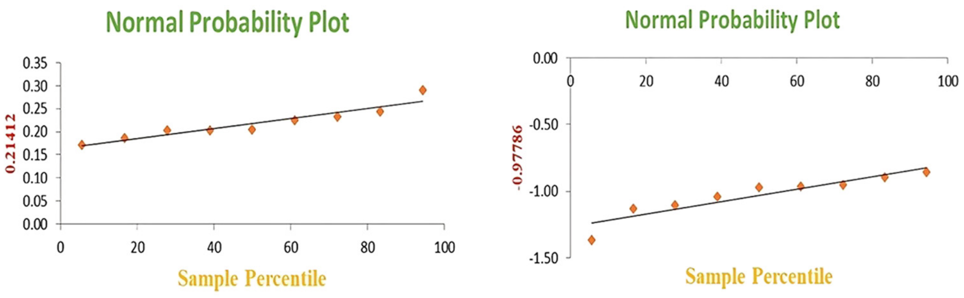

Figure 22: Probability plot for skin friction of hybrid nanofluid 1 when the NSS and SHS are heated.

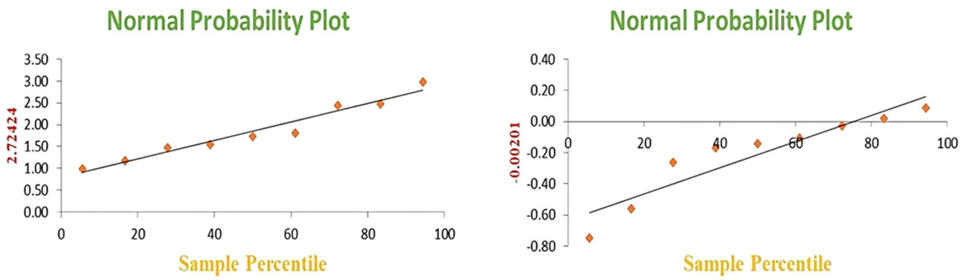

Figure 23: Probability plot for Nusselt number of hybrid nanofluid 1 when the NSS and SHS are heated.

$$
\begin{aligned}
U_2 = & -\frac{1{,}057}{1{,}342{,}042}Y^6-\frac{2{,}895}{205{,}228}Y^5-\frac{10{,}697}{205{,}510}Y^4 \\
& +\frac{10{,}732}{118{,}297}Y^3+\frac{9{,}679}{50{,}145}Y^2-\frac{17{,}333}{119{,}926}Y \\
& -\frac{5{,}570}{77{,}077}, \\
\theta_2 = & \frac{627}{772{,}045}Y^5+\frac{627}{308{,}818}Y^4-\frac{1{,}045}{154{,}409}Y^3 \\
& +\frac{1{,}568}{399{,}461}Y.
\end{aligned} \tag{36}
$$

For HNF-2 (a mixture of copper and graphene),

$$
U_0 = 0, \quad \theta_0 = \frac{2Y}{3}+\frac{1}{3}, \tag{37}
$$

$$
\begin{aligned}
U_1 = & -\frac{6{,}199}{165{,}186}Y^4-\frac{9{,}504}{50{,}651}Y^3-\frac{6{,}199}{27{,}531}Y^2 \\
& +\frac{25{,}207}{83{,}962}Y+\frac{12{,}398}{82{,}593}, \\
\theta_1 = & -\frac{15{,}321}{362{,}639}Y^3-\frac{48{,}395}{763{,}654}Y^2+\frac{15{,}929}{150{,}812}Y,
\end{aligned} \tag{38}
$$

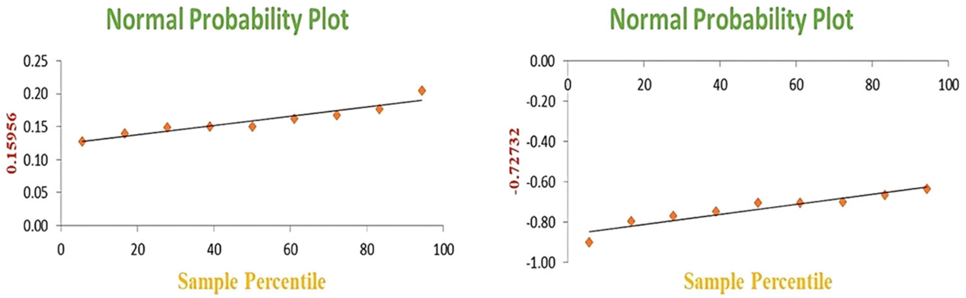

Figure 24: Probability plot for skin friction of hybrid nanofluid 2 when the NSS and SHS are heated.

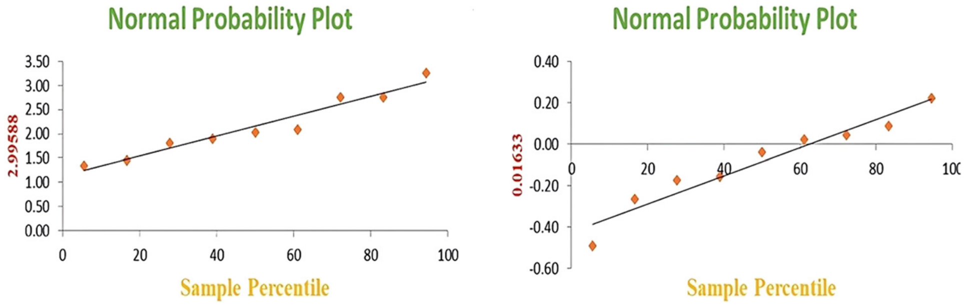

Figure 25: Probability plot for Nusselt number of hybrid nanofluid 2 when the NSS and SHS are heated.

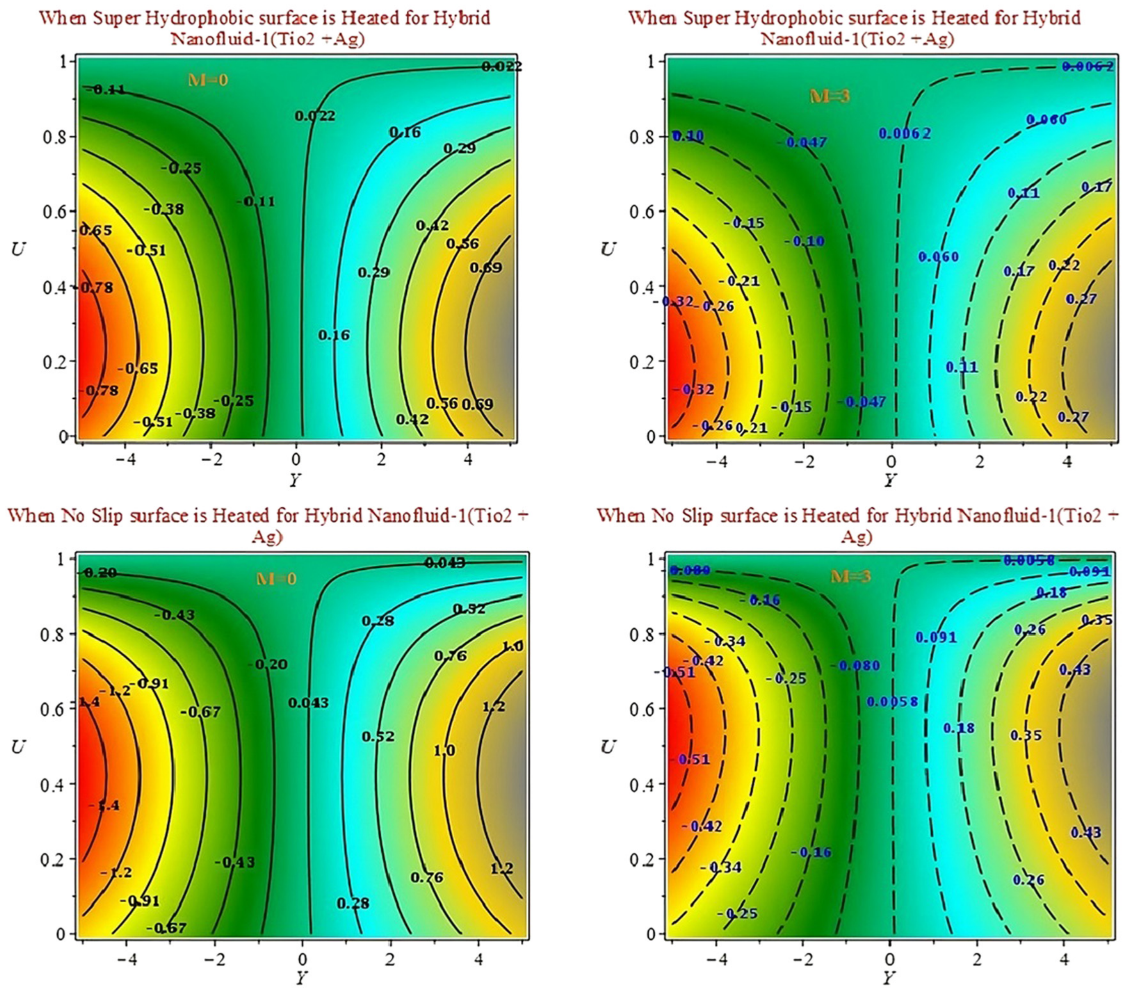

When Super Hydrophobic surface is Heated for Hybrid Nanofluid-1(Tio2 +Ag)

When Super Hydrophobic surface is Heated for Hybrid Nanofluid-1(Tio2 +Ag)

When No Slip surface is Heated for Hybrid Nanofluid-1(Tio2 + Ag)

When No Slip surface is Heated for Hybrid Nanofluid-1(Tio2 + Ag)

Figure 26: For hybrid nanofluid 1 variations in streamlines with *M* for fixed *N* = 1, Kp = 1, Ec = 1, Pr = 6.8, *R* = 1, Q_T = 1, λ = 0.5, and γ = 0.5.

$$\begin{aligned} U_2 &= -\frac{767}{1{,}216{,}041}Y^6 - \frac{8{,}597}{770{,}913}Y^5 - \frac{16{,}393}{400{,}098}Y^4 \\ &\quad + \frac{8{,}391}{117{,}185}Y^3 + \frac{10{,}620}{69{,}869}Y^2 - \frac{4{,}208}{36{,}945}Y \\ &\quad - \frac{2{,}104}{36{,}945}, \\ \theta_2 &= \frac{789}{982{,}289}Y^5 + \frac{863}{429{,}767}Y^4 - \frac{2{,}548}{380{,}665}Y^3 \\ &\quad + \frac{5{,}170}{1{,}331{,}699}Y. \end{aligned} \tag{39}$$

4 Result and discussion

In our research, numerous insights were gained through the meticulous computation of precise solutions and the generation of graphs using custom algorithms developed in the Maple program (Version 2018). We focused on two distinct hybrid nanofluids subjected to heating on two different surfaces, one with a no-slip condition and the other with a SHS. Our analysis primarily centered on investigating the impact of various parameters on temperature and velocity profiles. Additionally, we explored how these parameters affect bulk temperature, flow rate, streamlines, and isotherms. Furthermore, we utilized multilinear regression to analyze Nusselt number and skin friction data for different hybrid nanofluids.

Figure 2 showcases the pivotal role of the magnetic field parameter in influencing fluid dynamics. As this parameter increases, there is a notable escalation in velocity amplitude, indicating a stronger interaction between the liquid molecules and the magnetic field. This phenomenon holds significant implications, particularly in applications where controlling fluid motion is crucial, such as in magnetic drug targeting or magnetic resonance imaging.

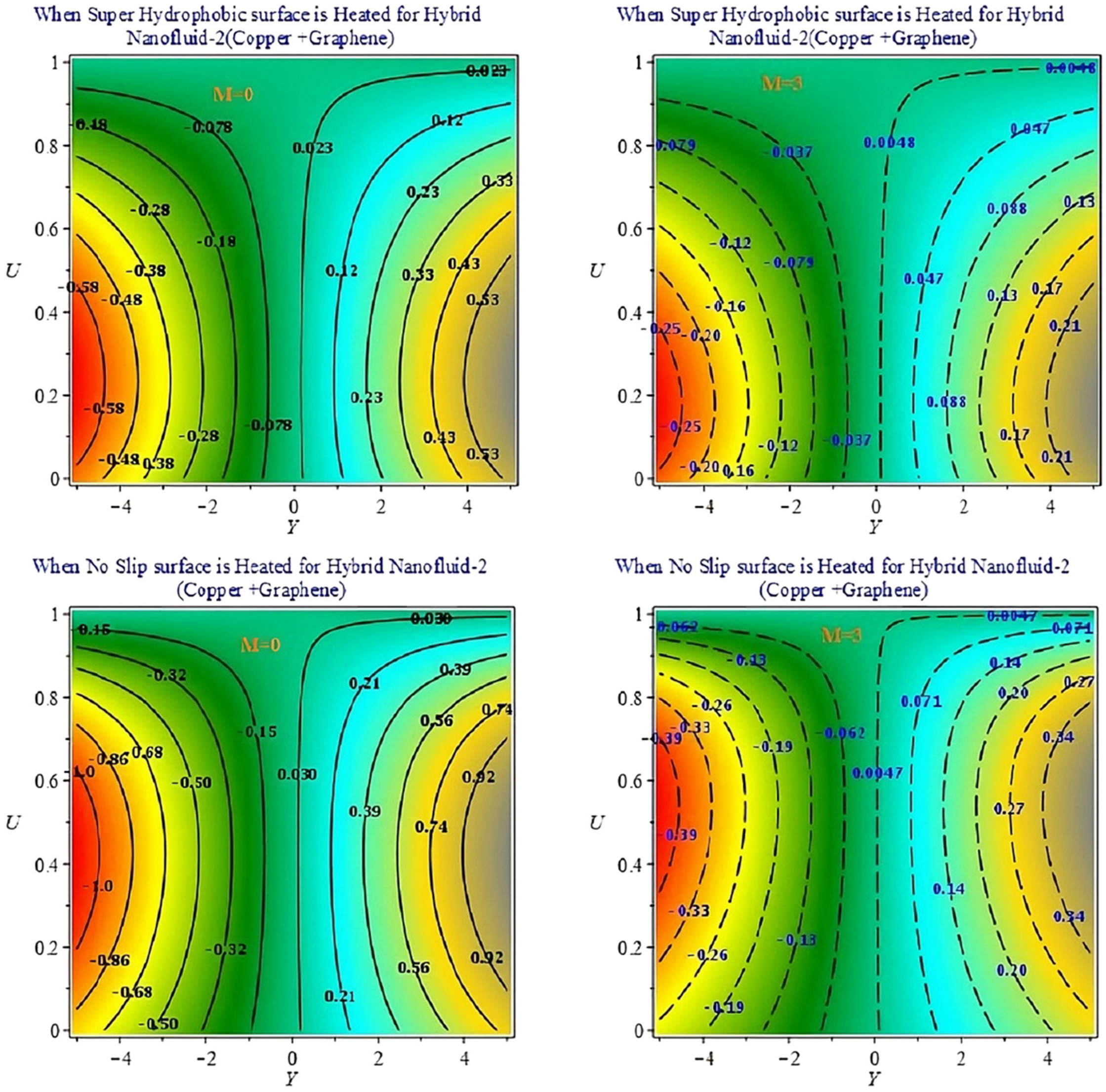
When Super Hydrophobic surface is Heated for Hybrid Nanofluid-2(Copper +Graphene)

When Super Hydrophobic surface is Heated for Hybrid Nanofluid-2(Copper +Graphene)

When No Slip surface is Heated for Hybrid Nanofluid-2 (Copper +Graphene)

When No Slip surface is Heated for Hybrid Nanofluid-2 (Copper +Graphene)

Figure 27: For hybrid nanofluid 2 variations in streamlines with M for fixed N = 1, Kp = 1, Ec = 1, Pr = 6.8, R = 1, Q_T = 1, λ = 0.5, and y = 0.5.

Moving to Figures 3 and 4, we delve into the intricacies of porosity parameters (Kp) and their impact on velocity and temperature profiles. Porous media, such as SHS and NSS, profoundly affect the fluid flow characteristics. An increase in Kp leads to expanded velocity and temperature profiles, emphasizing enhanced fluid movement and heat transfer within the system. This understanding is fundamental in optimizing the design of heat exchangers and porous media-based filtration systems. Now, turning to Figure 5, the variation of the Eckert number (Ec) sheds light on the thermal behavior of the system. A higher Ec signifies greater kinetic energy conversion into thermal energy, resulting in elevated temperatures, a vital consideration in applications like industrial cooling or thermal management systems. Figures 6 and 7 introduce the concept of the heat generation coefficient (Q_T), elucidating its role in influencing temperature and velocity profiles. A rise in Q_T prompts intensified heat generation and fluid motion, offering insights into optimizing heat transfer processes in engineering systems. Figure 8 delves into the impact of thermal radiation (R) on temperature profiles. Increasing R values lead to reduced temperatures, showcasing the cooling effect of thermal radiation, which is crucial in various applications ranging from electronic cooling to space exploration. Together, these figures provide a comprehensive understanding of the complex interplay between physical parameters and fluid behavior, guiding the design and optimization of diverse engineering systems.

Figures 9 and 10 present the velocity and temperature profiles for two distinct hybrid nanoparticles when the SHS

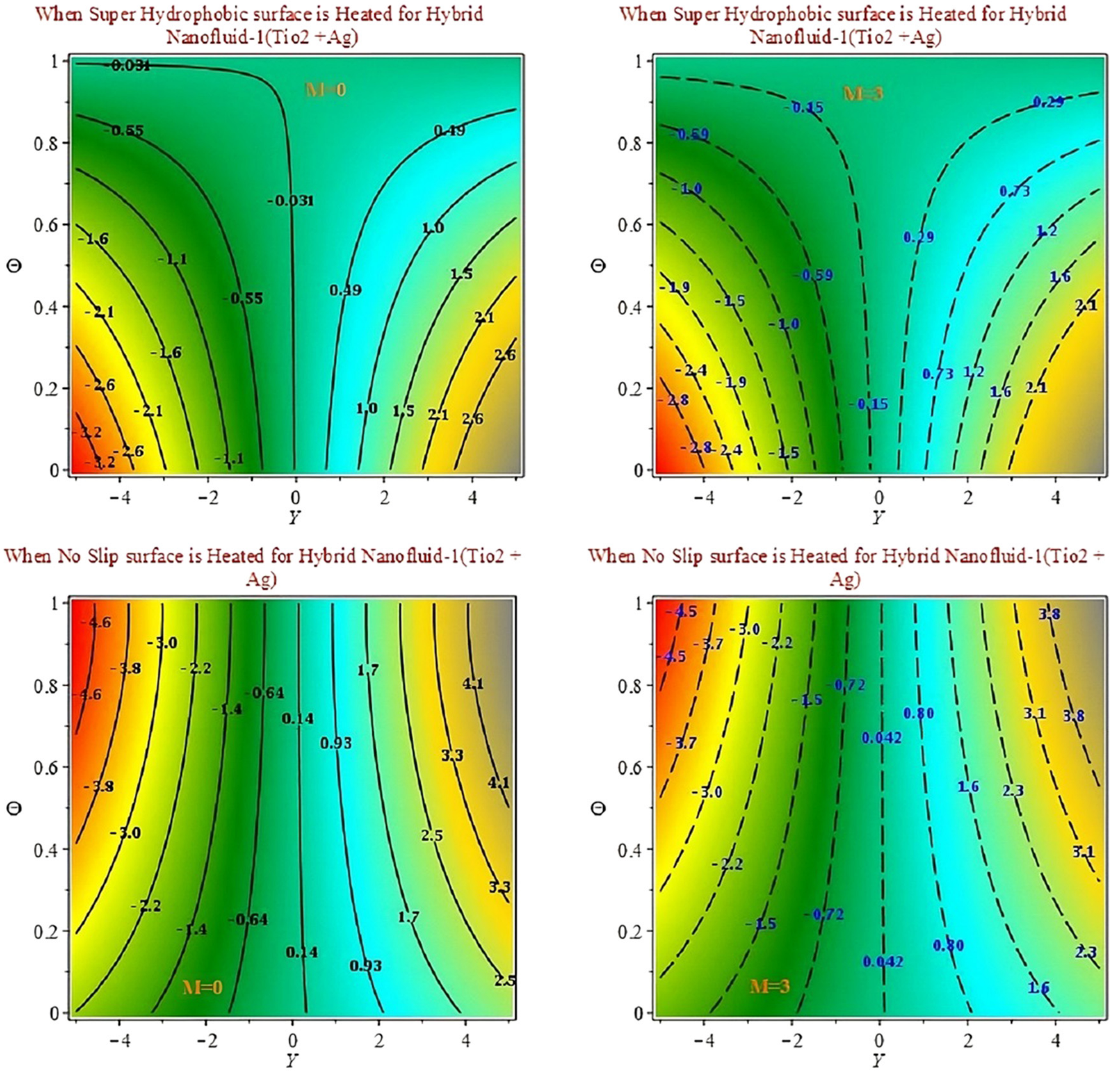

Figure 28: For hybrid nanofluid 1 variations in isotherms with M for fixed $N = 1$, $\mathrm{Kp} = 1$, $\mathrm{Ec} = 1$, $\mathrm{Pr} = 6.8$, $R = 1$, $Q_{\mathrm{T}} = 1$, $\lambda = 0.5$, and $\gamma = 0.5$.

and the NSS are heated, respectively. A noteworthy observation is that as the slip length value increases, both velocity and temperature profiles increase when either of the surfaces is heated. Figures 11 and 12 illustrate the temperature and velocity profiles for the same hybrid nanoparticles when the SHS and NSS are heated, respectively. When the temperature jump parameter increases, both velocity and temperature profiles increase when NSS is heated, but this trend is reversed when SHS is heated. The effect of the Prandtl number on the temperature profile is demonstrated in Figure 13. As the Prandtl number increases, the temperature profile also increases when both surfaces are heated. Figures 14 and 15 delve into the impact of the magnetic parameter (M) on volume flow rate and bulk temperature for different heated surfaces. In both cases, bulk temperature decreases and volume flow rate increases as the magnetic parameter increases for the two different hybrid nanofluids. Figures 16 and 17 showcase the influence of the porosity parameter (Kp) on volume flow rate and bulk temperature for different heated surfaces. Here, both bulk temperature and flow rate increase as the Kp value increases. Figure 18 further illustrates that in both scenarios, the bulk temperature increases as the Eckert number (Ec) increases. Figures 19 and 20 demonstrate how the heat generation coefficient (Q_{T}) affects the volume flow rate and bulk temperature for different heated surfaces, with both bulk temperature and flow rate rising as Q_{T} increases. Finally, Figure 21 indicates that in both situations, the bulk temperature decreases as the radiation parameter increases. Transitioning to probabilistic analyses, Figure 22 presents the probability plots of skin friction, and Figure 23 illustrates the probability

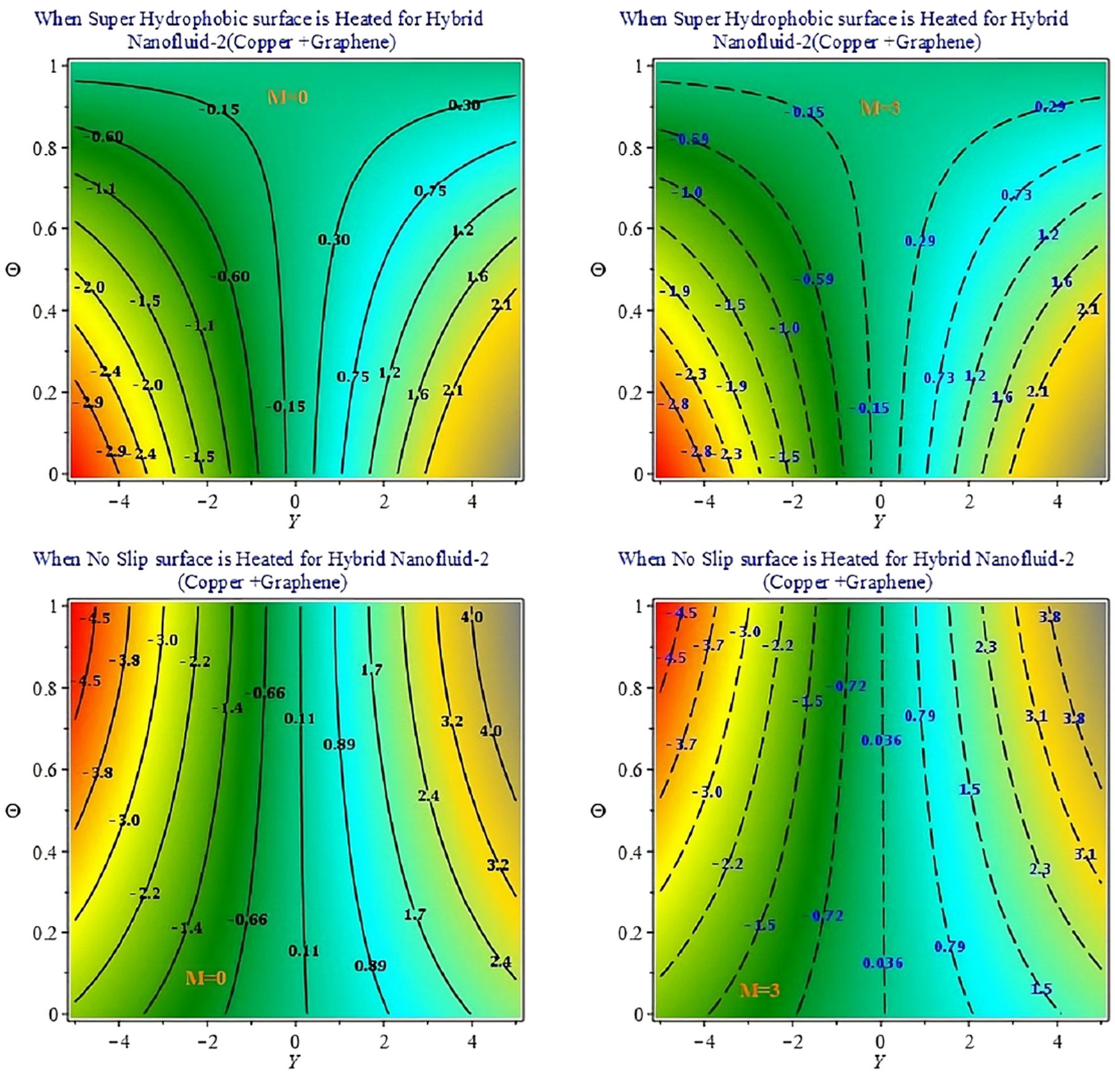

Figure 29: For hybrid nanofluid 2 variations in isotherms with M for fixed $N = 1$, Kp = 1, Ec = 1, Pr = 6.8, $R = 1$, $Q_T = 1$, $\lambda = 0.5$, and $\gamma = 0.5$.

plots of the Nu for two scenarios involving a mixture of TiO_2 and silver nanoparticles, with SHS and NSS heating, respectively. Similarly, Figure 24 shows the probability plots of skin friction, and Figure 25 shows the probability plots of the Nu for two cases involving a mixture of copper and graphene nanoparticles with SHS and NSS heating. Streamlines and isotherms are essential in fluid dynamics and heat transfer studies as they provide critical insights into flow patterns and temperature distributions. Streamlines illustrate the paths of fluid particles, helping identify flow characteristics such as laminar or turbulent regions, separation zones, and areas of high velocity or stagnation. This understanding is vital for optimizing designs in systems such as heat exchangers and aerodynamic structures. Isotherms, which connect points of equal temperature, reveal temperature gradients and heat distribution, which are crucial for effective thermal management and preventing overheating or inefficiencies. Together, these visualizations aid in performance evaluation, design optimization, and troubleshooting by highlighting flow behavior and thermal patterns, ultimately leading to more efficient and reliable engineering systems. Figures 26–29 depict the streamlines and isotherms with and without magnetic parameters for both TiO_2 and silver nanoparticles and copper and graphene nanoparticles when SHS and NSS are heated. These comprehensive analyses provide valuable insights into the complex interactions and behaviors of hybrid nanofluids under various heating conditions and parameter variations. Figure 30(a)–(d) depicts the contour plots of Cf with the magnetic parameter M *versus* Ec, Kp, R, Q_T having a different combination of hybrid nanofluid when a SHS is heated and the NSS is heated. Skin friction will increase for the increasing

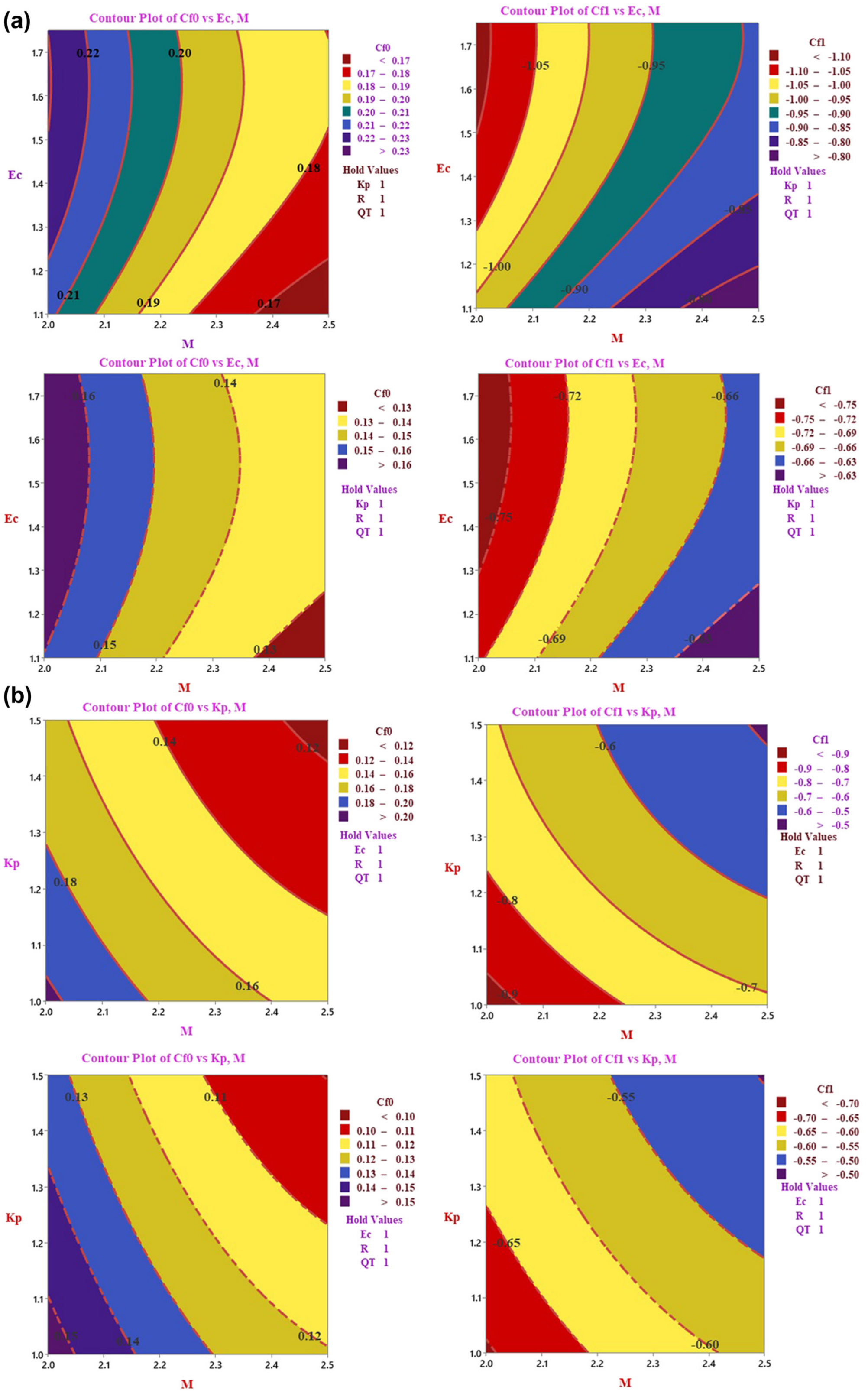

Figure 30: (a) For hybrid nanofluid 1 and 2 contour plot of skin friction for *M versus* Ec when the SHS and NSS are heated; (b) for hybrid nanofluids 1 and 2 contour plot of skin friction for *M versus* Kp when the SHS and NSS are heated; (c) for hybrid nanofluids 1 and 2 contour plot of skin friction for *M versus R* when the SHS and NSS are heated; and (d) for hybrid nanofluids 1 and 2 contour plot of skin friction for *M versus* Q_T when the SHS and NSS are heated.

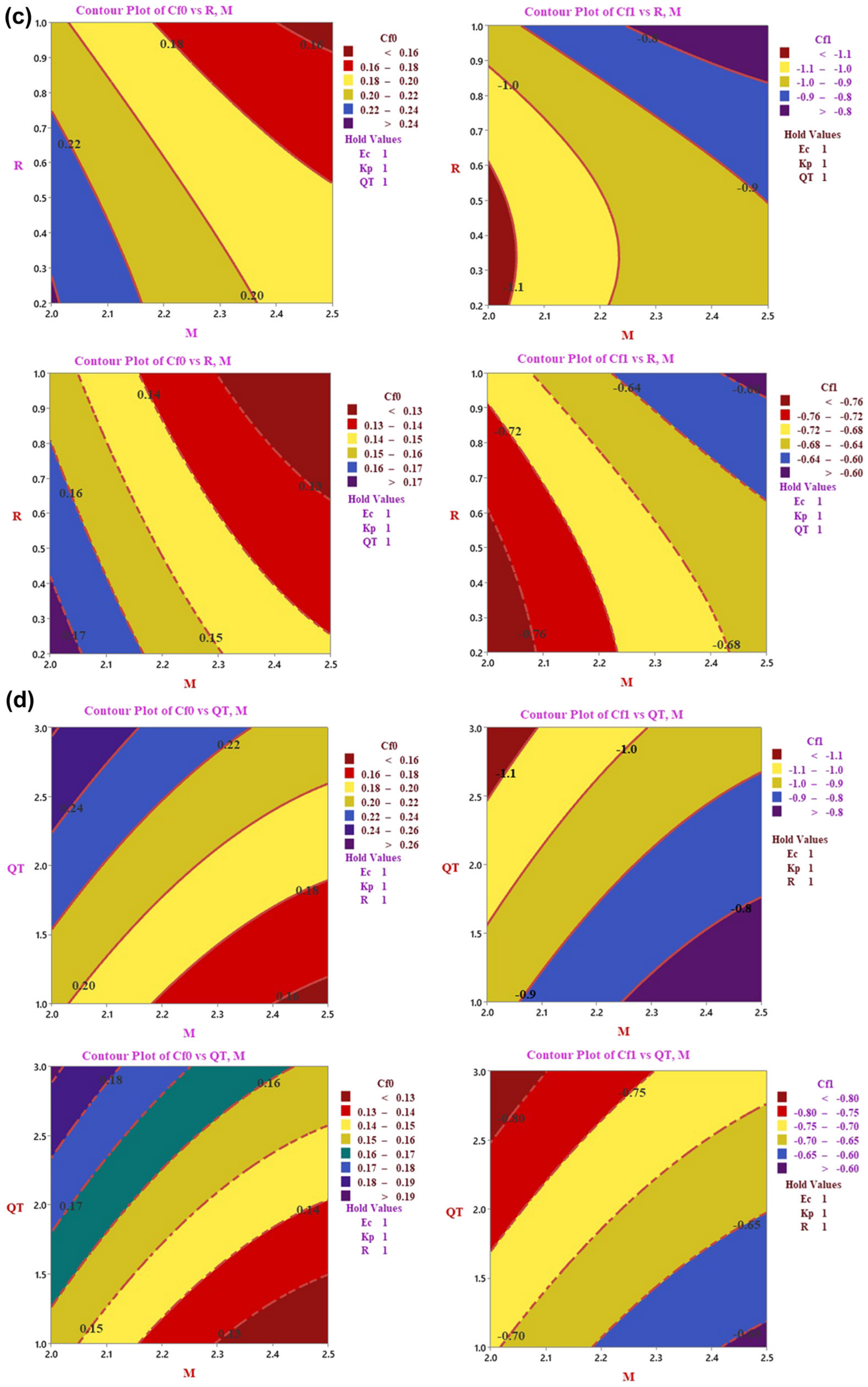

Figure 30: (*Continued*)

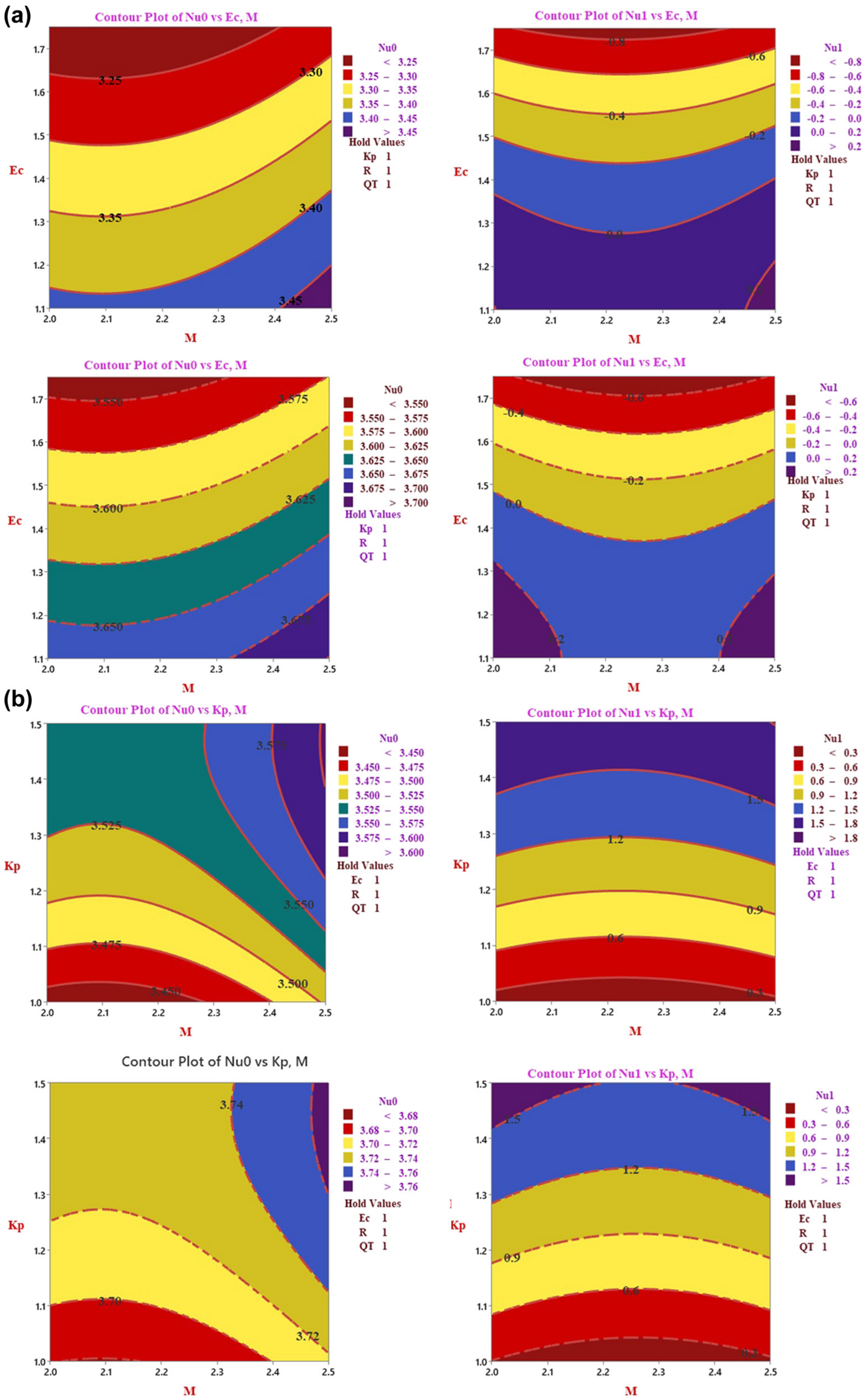

Figure 31: (a) for hybrid nanofluids 1 and 2 contour plot of Nusselt number for *M versus* Ec when the SHS and NSS are heated; (b) for hybrid nanofluids 1 and 2 contour plot of Nusselt number for *M versus* Kp when the SHS and NSS are heated; (c) for hybrid nanofluids 1 and 2 contour plot of Nusselt number for *M versus R* when the SHS and NSS are heated; and (d) for hybrid nanofluids 1 and 2 contour plot of Nusselt number for *M versus* Q_T when the SHS and NSS are heated.

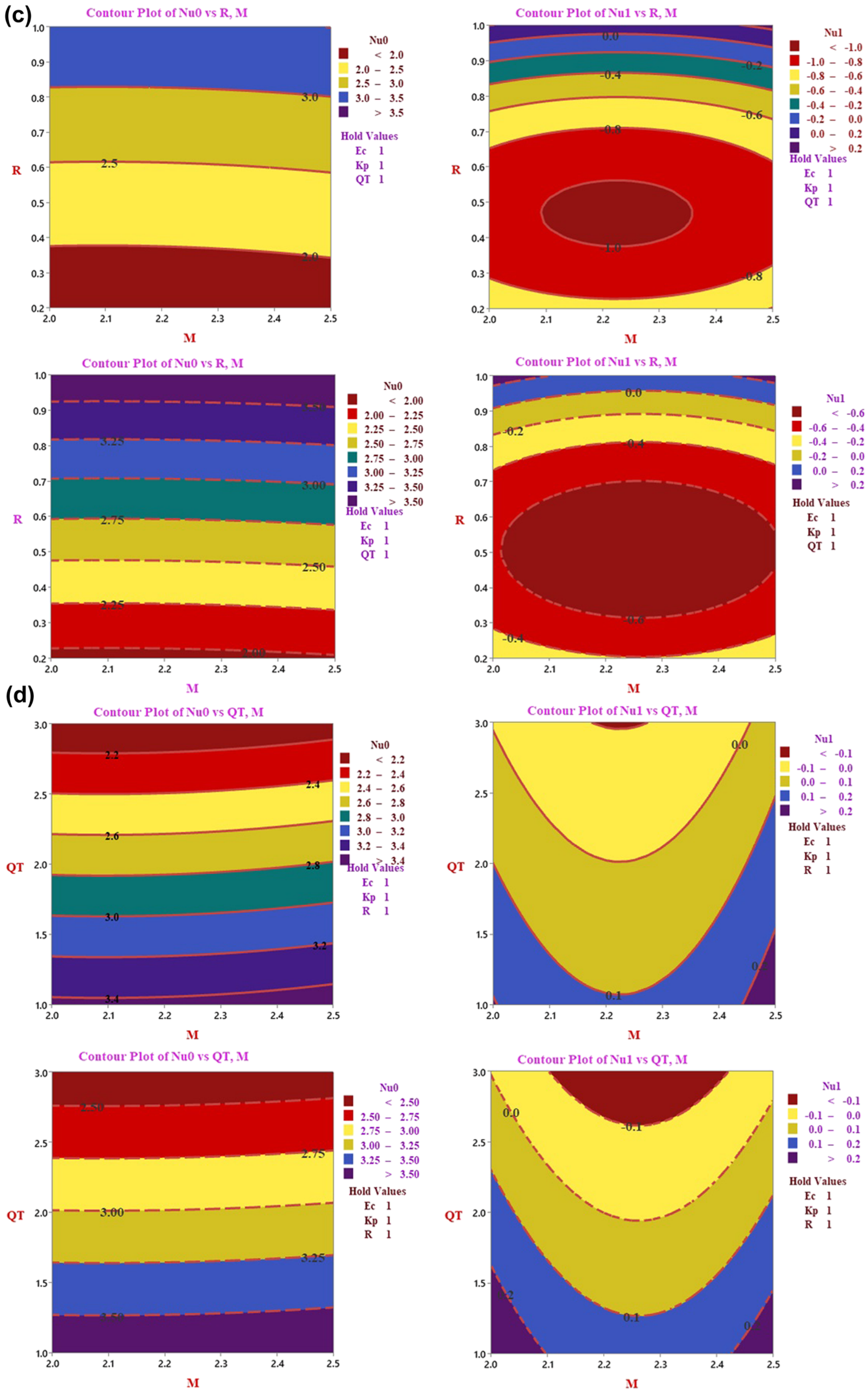

Figure 31: (*Continued*)

Table 1: Sources of nanoparticles include density, thermal conductivity, and specific heat capacity of water, as well as the kinds and forms of nanoparticles

	Nomenclature of nanoparticles and base fluid	**ρ (kg m^{-3})**	**Cp (kg K^{-1})**	**σ (μS cm^{-1})**	**k (W mk^{-1})**
Base fluid	Water H_2O	997.1	4,179	0.05	0.623
Hybrid nanofluid 1	TiO_2	4,250	686.2	2.38×10^6	8.9538
	Silver Ag	10,500	235	3.5×10^6	429
Hybrid nanofluid 2	Copper Cu	8,933	385	5.96×10^7	401
	Graphene	2,200	790	10^7	5,000

Table 2: Comparison of parameter values with the past study findings

Variables and parameters	**Present work Y = 0.5, N = 0, Kp = 0, Ec = 0, Pr = 0, Y = 1, M = 1, λ = 1**	**Jha and Gwandu [22] Y = 0.5, M = 1, N = 0, Y = 1, λ = 1**	**Variables and parameters**	**Present work Y = 0.5, N = 0, Kp = 0, Ec = 0, Pr = 0, Y = 1, M = 1, λ = 1**	**Jha BK and Gwandu [22] Y = 0.5, M = 1, N = 0, Y = 1, λ = 1**
Type I: SHS is heated			**Type II: NSS is heated**		
τ_0	0.067668	0.0677	τ_1	−0.500000	−0.5000
Nu_0	1.602604	1.6026	Nu_1	0.707277	0.7073
θ_b	0.311992	0.3120	θ_b	0.706937	0.7069
Q	0.050212	0.0502	Q	0.117879	0.1179
U	0.058300	0.0583	U	0.143469	0.1435

Table 3: Variation of the following physical parameters when SHS is heated: skin friction, Nusselt number, volume flow rate, and bulk temperature of hybrid nanoparticle 1 (combination of TiO_2 and silver Ag) and hybrid nanoparticle 2 (combination of copper and graphene) (M = 2, N = 1, λ = 0.5, γ = 0.5, Ec = 1, Kp = 1, R = 1, Q_T = 1, Pr = 6.8, A = 1, B = 0)

							Hybrid nanofluid 1				**Hybrid nanofluid 2**				
Case-1 (SHS heated)							R	M	Ec	Kp	Q_T	λ	γ	Cf_0	$\mathrm{Nu}_0\theta_pQ\mathrm{Cf}_0\mathrm{Nu}_0\theta_pQ$
0.1							0.23212	1.44907	0.49975	0.07819	0.16992	1.72776	0.48496	0.05394	
0.5							0.21665	2.31513	0.47294	0.07245	0.16133	2.58641	0.46522	0.05093	
1							0.20763	3.38735	0.45703	0.06911	0.15588	3.65479	0.45252	0.04903	
	2.1						0.20010	3.39388	0.45698	0.06626	0.15031	3.65757	0.45269	0.04704	
	2.3						0.18582	3.40432	0.45704	0.06088	0.13973	3.66125	0.45315	0.04327	
	2.5						0.17261	3.41160	0.45730	0.05593	0.12991	3.66270	0.45375	0.03979	
		1.1					0.20809	3.37273	0.45787	0.06929	0.15610	3.64481	0.45305	0.04911	
		1.4					0.20950	3.32834	0.46044	0.06984	0.15677	3.61463	0.45467	0.04936	
		1.8					0.21146	3.26780	0.46400	0.07059	0.15769	3.57381	0.45688	0.04970	
			1.1				0.20413	3.37949	0.45761	0.06778	0.15321	3.64857	0.45299	0.04807	
			1.3				0.19657	3.36358	0.45882	0.06491	0.14746	3.63578	0.45399	0.04601	
			1.5				0.18843	3.34805	0.46007	0.06183	0.14129	3.62302	0.45504	0.04381	
				1			0.20763	3.38735	0.45703	0.06911	0.15588	3.65479	0.45252	0.04903	
				3			0.25898	2.04586	0.54424	0.08798	0.19083	2.33258	0.53119	0.06116	
				5			0.34799	0.65336	0.68152	0.12104	0.24734	0.98172	0.64799	0.08096	
					0.2		0.30539	3.50173	0.44223	0.05613	0.22946	3.77581	0.43809	0.03986	
					0.5		0.20763	3.38735	0.45703	0.06911	0.15588	3.65479	0.45252	0.04903	
					0.8		0.15761	3.33007	0.46355	0.07596	0.11819	3.59997	0.45858	0.05383	
						0.1	0.30469	3.29122	0.60407	0.10080	0.22945	3.58458	0.59942	0.07167	
						0.3	0.24798	3.34836	0.52085	0.08230	0.18633	3.62626	0.51603	0.05842	
						0.5	0.20763	3.38735	0.45703	0.06911	0.15588	3.65479	0.45252	0.04903	

Table 4: Variation of the following physical parameters when NSS is heated: skin friction, Nusselt number, volume flow rate, and bulk temperature of hybrid nanoparticle 1 (combination of TiO_2 and silver Ag) and hybrid nanoparticle 2 (combination of copper and graphene) (M = 2, N = 1, λ = 0.5, γ = 0.5, Ec = 1, Kp = 1, R = 1, Q_T = 1, Pr = 6.8, A = 0, B = 1)

Case 2 (NSS heated)							**Hybrid nanofluid 1**				**Hybrid nanofluid 2**			
R	M	Ec	Kp	Q_T	λ	γ	Cf_1	Nu_1	θ_p	Q	Cf_1	Nu_1	θ_p	Q
0.1							−1.06154	−0.26070	0.79210	0.15348	−0.76823	0.11219	0.75382	0.10258
0.5							−0.99094	−0.10285	0.73741	0.13800	−0.73462	0.26333	0.71869	0.09557
1							−0.95367	−0.02085	0.70785	0.12989	−0.71425	0.4666	0.69708	0.09134
	2.1						−0.92959	−0.02180	0.70687	0.12450	−0.69697	0.04768	0.69684	0.08769
	2.3						−0.88393	−0.02350	0.70545	0.11442	−0.66398	0.04950	0.69668	0.08079
	2.5						−0.84156	−0.02493	0.70462	0.10523	−0.63314	0.05104	0.69689	0.07445
		1.1					−0.95707	−0.01931	0.71041	0.13058	−0.71581	0.04496	0.69864	0.09165
		1.4					−0.96779	−0.01456	0.71847	0.13276	−0.72064	0.03976	0.70345	0.09257
		1.8					−0.98345	−0.00790	0.73020	0.13597	−0.72744	0.03263	0.71020	0.09388
			1.1				−0.94339	−0.02085	0.70908	0.12761	−0.70637	0.04665	0.69801	0.08968
			1.3				−0.92091	−0.02088	0.71160	0.12265	−0.68925	0.04668	0.69994	0.08609
			1.5				−0.89636	−0.02097	0.71409	0.11727	−0.67066	0.04676	0.70190	0.08223
				1			−0.95367	0.02085	0.70785	0.12989	−0.71425	0.04666	0.69708	0.09134
				3			−1.12626	−0.01859	0.84550	0.16931	−0.82597	−0.0154	0.81595	0.11549
				5			−1.47766	−0.06249	1.10025	0.25272	−1.01782	−0.0789	1.00613	0.15851
					0.2		−0.93007	−0.02084	0.72446	0.11493	−0.69655	0.04615	0.71313	0.08076
					0.5		−0.95367	−0.02085	0.70785	0.12989	−0.71425	0.04666	0.69708	0.09134
					0.8		−0.96674	−0.02059	0.70151	0.13778	−0.72376	0.04660	0.69068	0.09687
						0.1	−0.80630	−0.06021	0.56265	0.08999	−0.60862	0.11242	0.55863	0.06404
						0.3	−0.88581	−0.03642	0.64091	0.11128	−0.66619	0.07243	0.63385	0.07875
						0.5	−0.95367	−0.02085	0.70785	0.12989	−0.71425	0.04666	0.69708	0.09134

Table 5: Skin friction and Nusselt number of hybrid nanoparticle 1 (combination of TiO_2 and silver Ag) and hybrid nanoparticle 2 (combination of copper and graphene) for different physical parameters are examined when SHS is heated (N = 1, λ = 0.5, γ = 0.5, Pr = 6.8, A = 1, B = 0)

					HNF 1		**HNF 2**		
Case 1 (SHS heated)					M	Ec	Kp	R	$Q_TCf_0Nu_0Cf_0Nu_0$
2.2	1.1	1	1	2	0.21412	2.72424	0.15956	2.99588	
2.45	1.5	1.4	0.6	1	0.17219	2.47117	0.12819	2.75164	
2.3	1.2	1.25	0.4	1.5	0.20517	1.74115	0.15084	2.02273	
2.15	1.7	1.5	0.7	2.5	0.23190	1.54775	0.16720	1.89742	
2.2	1.6	1.35	0.8	3	0.24425	1.47138	0.17631	1.80967	
2.4	1.15	1.05	0.2	1.75	0.22521	1.16912	0.16287	1.44944	
2.35	1.3	1.1	0.9	1.25	0.18670	2.98695	0.13968	3.25714	
2.15	1.75	1.45	0.85	1.7	0.20273	2.44239	0.14946	2.76396	
2.5	1.15	1.2	0.65	2.25	0.20343	1.80909	0.14981	2.08224	
2	1.4	1.15	0.5	2.75	0.29074	0.98705	0.20550	1.33718	

values of Ec, Q_T when SHS is heated but it will decrease when the NSS is heated. We can observe the opposite behavior for the parameters Kp, R. Similarly, Figure 31(a–d) gives the contour plots of the Nu with the magnetic parameter M *versus* Ec, Kp, R, Q_T having a different combination of hybrid nanofluid when a SHS is heated and the NSS is heated. If either of the surfaces is heated, Nusselt number will decrease for Kp and Q_T, but for the Ecart number, the Nusselt number will decrease when SHS is heated and reverse when NSS is heated (Tables 1–6).

The adjusted-R^2 values presented in Tables 7(a) and 8(a) indicate that the regression model accurately

Table 6: Skin friction and Nusselt number of hybrid nanoparticle 1 (combination of TiO_2 and silver Ag) and hybrid nanoparticle 2 (combination of copper and graphene) for different physical parameters are examined when NSS is heated. ($N = 1$, $\lambda = 0.5$, $\gamma = 0.5$, $Pr = 6.8$, $A = 0$, $B = 1$)

Case 2 (NSS heated)					**HNF 1**		**HNF 2**	
M	**Ec**	**Kp**	R	Q_T	$\mathbf{Cf_1}$	$\mathbf{Nu_1}$	$\mathbf{Cf_1}$	$\mathbf{Nu_1}$
2.2	1.1	1	1	2	−0.97786	−0.00201	−0.72732	0.01633
2.45	1.5	1.4	0.6	1	−0.85456	0.08517	−0.63375	0.22341
2.3	1.2	1.25	0.4	1.5	−0.96675	−0.14350	−0.70664	0.04357
2.15	1.7	1.5	0.7	2.5	−1.10411	−0.26126	−0.77212	−0.17478
2.2	1.6	1.35	0.8	3	−1.13201	−0.16958	−0.79756	−0.15579
2.4	1.15	1.05	0.2	1.75	−1.04293	−0.55959	−0.74719	−0.26460
2.35	1.3	1.1	0.9	1.25	−0.89282	0.02123	−0.66654	0.08803
2.15	1.75	1.45	0.85	1.7	−0.96815	−0.02617	−0.70617	0.02265
2.5	1.15	1.2	0.65	2.25	−0.95159	−0.10772	−0.69981	−0.03835
2	1.4	1.15	0.5	2.75	−1.36400	−0.74792	−0.90234	−0.49370

represents the datasets for the skin friction coefficient (Cf) and Nusselt number (Nu) when both the SHS and NSS were heated for the mixture of TiO2 and silver nanoparticles. This indicates the model's robustness in capturing the physical phenomena of heat transfer and frictional forces under these conditions. Similarly, Tables 9(a) and 10(a) demonstrate that the model accurately predicts Cf and Nu for the mixture of copper and graphene nanoparticles under heated surface conditions, affirming its applicability across different hybrid nanofluids. The statistical significance of the model is further supported by the *P*-values of the *F*-test, which are all less than 0.05, indicating that the regression model is highly significant for predicting Nusselt number and skin friction for both hybrid nanoparticle types in scenarios where SHS and NSS are heated, as presented in Tables 7(b), 8(b), 9(b) and 10(b). This signifies the reliability of the model in explaining the variability in the data due to the predictor variables. Regression coefficients for Cf of hybrid nanoparticles 1 and 2 are detailed in Tables 7(c) and 9(c), respectively. For SHS heating, the parameters Eckert number (Ec), porosity parameter (Kp), and radiation parameter (R) are statistically insignificant (*P*-values greater than 0.05) in the *t*-test. This suggests that these parameters do not significantly influence skin friction under SHS conditions, which might be due to the dominance of other factors such as magnetic field and heat generation. On the other hand, the magnetic parameter (M) and heat generation coefficient (Q_T) are statistically significant (*P*-values less than 0.05), indicating their substantial impact on skin friction. The significance of M underscores the role of magnetic fields in modifying the flow and frictional characteristics of nanofluids, while Q_T highlights the effect of internal heat generation on skin friction. For NSS heating, the parameter Q_T remains statistically significant (*P*-values < 0.05) for hybrid nanoparticle 1, emphasizing the critical role of heat generation in affecting skin friction in no-slip conditions. For hybrid nanoparticle 2, both Q_T and M are statistically significant, reflecting the combined effects of magnetic fields and heat generation in influencing skin friction under NSS conditions. Based on the *P*-values (>0.05), the parameters M, Ec, Kp, and R are statistically insignificant in the *t*-test for hybrid nanoparticle 1, and for hybrid nanoparticle 2, Ec, Kp, and R are statistically insignificant. The regression coefficients for the Nusselt numbers of hybrid nanoparticles 1 and 2 are shown in Tables 8(c) and 10(c), respectively. When either surface is heated for hybrid nanoparticle 2, the parameter Q_T is statistically significant in the *t*-test, while the parameters Ec and Kp are statistically insignificant. For hybrid nanoparticle 1, when the SHS is heated, the parameter Kp is statistically insignificant in the *t*-test, whereas the parameters Ec, Q_T, M, and R are statistically significant. Similarly, when the NSS is heated, the parameter Q_T is statistically significant in the *t*-test, while the parameters M, Ec, Kp, and R are statistically insignificant. This statistical analysis highlights the varying influence of different parameters on the Nusselt number depending on the type of hybrid nanoparticle and the surface condition. For hybrid nanoparticle 2, Q_T significantly impacts the heat transfer characteristics under all conditions, indicating the critical role of heat generation in these systems. Conversely, parameters such as Ec and Kp do not show significant influence, suggesting that viscous dissipation and porosity might not be as impactful in these scenarios. For hybrid nanoparticle 1, the significance of M, Ec, Q_T, and R, when the SHS is heated, underscores the complex interaction between magnetic fields, viscous heating, heat generation, and thermal radiation in influencing heat transfer. However, when the NSS is heated, only Q_T remains significant, highlighting heat generation as a

Table 7: (a) When two different surfaces are heated, the regression statistics for skin friction of hybrid nanoparticle 1 (mixture of TiO_2, and silver Ag); (b) analysis of variance (ANOVA) for skin friction of hybrid nanoparticle 1 (a mixture of TiO_2, and silver Ag) when two different surfaces are heated; (c) when two different surfaces are heated, the regression coefficients for skin friction of hybrid nanoparticle 1 (a mixture of TiO_2, and silver Ag); and (d) PROBABILITY OUTPUT for skin friction of hybrid nanoparticle 1 (a mixture of TiO_2 and silver Ag) when two different surfaces are heated

(a)

	NSS	SHS
Multiple R	0.98161	0.99234
R^2	0.96355	0.98473
Adjusted R^2	0.90281	0.95928
Standard error	0.04819	0.00710
Observations	9	9

(b)

	NSS					SHS			
	df	SS	MS	F	Significance F	SS	MS	F	Significance F
Regression	5	0.18422	0.03684	15.8630	0.02285	0.00976	0.00195	38.69303	0.00632
Residual	3	0.00697	0.00232			0.00015	0.00005		
Total	8	0.19119				0.00991			

(c)

	SHS						NSS					
	Coefficients	Standard error	t Stat	P-value	Lower 95%	Upper 95%	Coefficients	Standard error	t Stat	P-value	Lower 95%	Upper 95%
Intercept	0.48893	0.07712	6.33968	0.00794	0.24349	0.73436	−2.29938	0.52323	−4.39460	0.02183	−3.96453	−0.63423
$M = 2.2$	−0.10346	0.02793	−3.70421	0.03418	−0.19235	−0.0145	0.50015	0.18950	2.63931	0.07770	−0.10292	1.10321
$\mathrm{Ec} = 1.1$	0.02171	0.03459	0.62768	0.57474	−0.08838	0.13180	−0.10460	0.23469	−0.44570	0.68602	−0.85149	0.64229
$\mathrm{Kp} = 1$	−0.07524	0.03681	−2.04423	0.13350	−0.19238	0.04190	0.30018	0.24972	1.20206	0.31557	−0.49455	1.09492
$R = 1$	−0.04533	0.01506	−3.00924	0.05725	−0.09328	0.00261	0.20147	0.10221	1.97126	0.14327	−0.12379	0.52674
$Q_{\mathrm{T}} = 2$	0.02947	0.00453	6.50644	0.00737	0.01505	0.04388	−0.11679	0.03073	−3.8010	0.03198	−0.21457	−0.01901

(d)

	SHS	NSS
Percentile	0.21412	−0.97786
5.55555556	0.17219	−1.36400
16.6666667	0.18670	−1.13201
27.7777778	0.20273	−1.10411
38.8888889	0.20343	−1.04293
50	0.20517	−0.96815
61.1111111	0.22521	−0.96675

(Continued)

Table 7: *Continued*

(d)		
	SHS	**NSS**
72.2222222	0.23190	−0.95159
83.3333333	0.24425	−0.89282
94.4444444	0.29074	−0.85456

Table 8: (a) Regression statistics for Nusselt number of hybrid nanoparticle 1 (a mixture of TiO_2 and silver Ag) when two different surfaces are heated; (b) when two different surfaces are heated, the ANOVA for Nusselt number of hybrid nanoparticle 1 (a mixture of TiO_2 and silver Ag); (c) when two different surfaces are heated, the regression coefficients for Nusselt number of hybrid nanoparticle 1 (a mixture of TiO_2 and silver Ag); and (d) when two different surfaces are heated, the PROBABILITY OUTPUT for Nusselt number of hybrid nanoparticle 1 (a mixture of TiO_2 and silver Ag)

(a)		
	SHS	**NSS**
Multiple *R*	0.99993	0.97744
R^2	0.99985	0.95538
Adjusted R^2	0.99961	0.88101
Standard error	0.01301	0.09487
Observations	9	9

(b)									
	SHS					**NSS**			
	df	**SS**	**MS**	***F***	**Significance *F***	**SS**	**MS**	***F***	**Significance *F***
Regression	5	3.48537	0.69707	4117.414	0.00001	0.57806	0.11561	12.8465	0.03073
Residual	3	0.00051	0.00017			0.02700	0.00900		
Total	8	3.48588				0.60506			

(c)												
	SHS						**NSS**					
	Coefficients	**Standard error**	***t* Stat**	***P*-value**	**Lower 95%**	**Upper 95%**	**Coefficients**	**Standard Error**	***t* Stat**	***P*-value**	**Lower 95%**	**Upper 95%**
Intercept	1.74271	0.14126	12.33665	0.00115	1.29315	2.19228	−2.24529	1.02994	−2.18002	0.11735	−5.5230	1.03244
$M = 2.2$	0.19483	0.05116	3.80818	0.03183	0.03201	0.35765	0.51024	0.37301	1.36788	0.26480	−0.6768	1.69733
$\mathrm{Ec} = 1.1$	−0.19105	0.06336	−3.01515	0.05698	−0.39269	0.01060	−0.55191	0.46197	−1.19469	0.31805	−2.0221	0.91828
$\mathrm{Kp} = 1$	−0.04644	0.06742	−0.68887	0.54040	−0.26101	0.16812	1.13299	0.49157	2.30486	0.10452	−0.4313	2.69737

(Continued)

Table 8: *Continued*

(c)

	SHS						NSS					
	Coefficients	**Standard error**	***t* Stat**	***P*-value**	**Lower 95%**	**Upper 95%**	**Coefficients**	**Standard Error**	***t* Stat**	***P*-value**	**Lower 95%**	**Upper 95%**
$R = 1$	2.17244	0.02759	78.72930	0.000005	2.08463	2.26026	0.81219	0.20118	4.03705	0.02734	0.17193	1.45245
$Q_{\mathrm{T}} = 2$	−0.69212	0.00830	−83.4343	0.000004	−0.71852	−0.66572	−0.14948	0.06048	−2.4715	0.08994	−0.3419	0.04300

(d)

	SHS	NSS
Percentile	2.72424	−0.00201
5.5555556	0.98705	−0.74792
16.666667	1.16912	−0.55959
27.777778	1.47138	−0.26126
38.888889	1.54775	−0.16958
50	1.74115	−0.14350
61.111111	1.80909	−0.10772
72.222222	2.44239	−0.02617
83.333333	2.47117	0.02123
94.444444	2.98695	0.08517

Table 9: (a) When two different surfaces are heated, the regression statistics for skin friction of hybrid nanoparticle-2 (mixture of copper and graphene). (b) When two different surfaces are heated, ANOVA for skin friction of hybrid nanoparticle-2 (mixture of copper and graphene). (c) When two different surfaces are heated the regression coefficients for skin friction of hybrid nanoparticle-2 (mixture of copper and graphene). (d) When two different surfaces are heated PROBABILITY OUTPUT for skin friction of hybrid nanoparticle-2 (mixture of copper and graphene)

(a)

	SHS	**NSS**
Multiple *R*	0.99396	0.99199
R^2	0.98795	0.98404
Adjusted R^2	0.96786	0.95743
Standard error	0.00406	0.01651
Observations	9	9

(b)

	SHS					**NSS**			
	d*f*	**SS**	**MS**	***F***	**Significance *F***	**SS**	**MS**	***F***	**Significance *F***
Regression	5	0.00406	0.00081	49.1748	0.00445	0.05040	0.01008	36.99	0.00675
Residual	3	0.00005	0.00002			0.00082	0.00027		
Total	8	0.00411				0.05122			

(c)

	SHS						**NSS**					
	Coefficients	**Standard error**	***t* Stat**	***P*-value**	**Lower 95%**	**Upper 95%**	**Coefficients**	**Standard error**	***t* Stat**	***P*-value**	**Lower 95%**	**Upper 95%**
Intercept	0.34031	0.04411	7.71473	0.00453	0.19993	0.48069	−1.36773	0.17924	−7.63078	0.00467	−1.93815	−0.79732
$M = 2.2$	−0.06875	0.01598	−4.30363	0.02309	−0.11960	−0.01791	0.24721	0.06492	3.80815	0.03183	0.04062	0.45380
$\mathrm{Ec} = 1.1$	0.01084	0.01979	0.54794	0.62187	−0.05213	0.07381	−0.04870	0.08040	−0.60574	0.58745	−0.30456	0.20716
$\mathrm{Kp} = 1$	−0.04828	0.02105	−2.29343	0.10562	−0.11529	0.01872	0.16114	0.08555	1.88361	0.15614	−0.11111	0.43338
$R = 1$	−0.02592	0.00862	−3.00770	0.05732	−0.05334	0.00151	0.09665	0.03501	2.76039	0.070130	−0.01478	0.20807
$Q_{\mathrm{T}} = 2$	0.01900	0.00259	7.3348	0.00524	0.01076	0.02724	−0.06529	0.01053	−6.20276	0.008443	−0.09878	−0.03179

(d)

	SHS	**NSS**
Percentile	0.15956	−0.72732
5.5555556	0.12819	−0.90234
16.666667	0.13968	−0.79756
27.777778	0.14946	−0.77212
38.888889	0.14981	−0.74719

(Continued)

Table 9: *Continued*

(d)		
	SHS	**NSS**
50	0.15084	−0.70664
61.111111	0.16287	−0.70617
72.222222	0.16720	−0.69981
83.333333	0.17631	−0.66654
94.444444	0.20550	−0.63375

Table 10: (a) When two different surfaces are heated regression statistics for Nusselt number of hybrid nanoparticle-2 (mixture of copper and graphene). (b) When two different surfaces are heated ANOVA for Nusselt number of hybrid nanoparticle-2 (mixture of copper and graphene). (c) When two different surfaces are heated, the regression coefficients for Nusselt number of hybrid nanoparticle-2 (mixture of copper and graphene). (d) When two different surfaces are heated, the PROBABILITY OUTPUT for Nusselt number of hybrid nanoparticle-2 (mixture of copper and graphene)

(a)

	SHS	NSS
Multiple *R*	0.99998	0.97929
R^2	0.99996	0.95901
Adjusted R^2	0.99988	0.89070
Standard Error	0.00702	0.07088
Observations	9	9

(b)

	SHS					NSS			
	df	SS	MS	*F*	Significance *F*	SS	MS	*F*	Significance *F*
Regression	5	3.31635	0.66327	13468.42	0.000001	0.35262	0.07052	14.04	0.02714
Residual	3	0.00015	0.00005			0.01507	0.00502		
Total	8	3.31650				0.36769			

(c)

	SHS						NSS					
	Coefficients	Standard Error	*t* Stat	*P*-value	Lower 95%	Upper 95%	Coefficients	Standard Error	*t* Stat	*P*-value	Lower 95%	Upper 95%
Intercept	2.11930	0.07619	27.81668	0.00010	1.87684	2.36177	−1.21045	0.76951	−1.57302	0.21377	−3.65937	1.23847
$M = 2.2$	0.10862	0.02759	3.93653	0.02920	0.02081	0.19644	0.32689	0.27869	1.17294	0.32548	−0.56004	1.21382
$\mathrm{Ec} = 1.1$	−0.12528	0.03417	−3.66613	0.03509	−0.23404	−0.01653	−0.44289	0.34516	−1.28316	0.28958	−1.54133	0.65555
$\mathrm{Kp} = 1$	−0.04153	0.03636	−1.14224	0.33626	−0.15726	0.07419	0.87167	0.36727	2.37339	0.09820	−0.29714	2.04048
$R = 1$	2.14690	0.01488	144.2579	0.000001	2.09953	2.19426	0.42607	0.15031	2.83457	0.065941	−0.05229	0.90444
$Q_{\mathrm{T}} = 2$	−0.67111	0.00447	−150.004	0.000001	−0.68535	−0.65688	−0.18511	0.04519	−4.09658	0.026308	−0.32892	−0.04131

(d)

	SHS	NSS
Percentile	2.99588	0.01633
5.5555556	1.33718	−0.49370
16.666667	1.44944	−0.26460
27.777778	1.80967	−0.17478
38.888889	1.89742	−0.15579
50	2.02273	−0.03835
61.111111	2.08224	0.02265

(Continued)

Table 10: *Continued*

(d)		
	SHS	**NSS**
72.222222	2.75164	0.04357
83.333333	2.76396	0.08803
94.444444	3.25714	0.22341

dominant factor in these conditions. This analysis provides valuable insights into how different physical parameters affect the thermal performance of hybrid nanofluids under varying surface conditions, aiding in the optimization and design of efficient thermal management systems.

5 Conclusion

In summary, a vertical microfree channel, the convective flow of an electrically conducting and incompressible hybrid nanofluid with porous media, was considered, and then, both surfaces were alternately heated. Across the channel, a transverse magnetic field was used. One of the channel walls was nonslip, whereas the other was extremely hydrophobic. The investigation's major goal is to determine how the flow's primary properties are impacted by superhydrophobicity, magnetism, wall porosity, and the thermal radiation effect. The following are a few findings that stand out:

1) The radiation parameter (R) decreases both the Nusselt number (Nu) and skin friction (Cf) for both hybrid nanofluids when NSS is heated, with an average percentage decrease of approximately 37.15% for Nu and approximately 5.21% for Cf but increases approximately 47.33% for Nu and decreases approximately 9.39% for Cf when SHS is heated. Similarly, it reduces the flow rate and bulk temperature when either of the surfaces is heated.
2) For hybrid nanofluids 1 and 2, the heat generation parameter decreases the Nusselt number and skin friction when the NSS is heated, whereas the values of skin friction rise at the SHS and drop at the NSS. Similarly, heat generation parameter increases the flow rate and bulk temperature when either of the surfaces is heated.
3) The velocity and temperature profile for both hybrid nanofluids will increases as the porosity parameter Kp and heat generation/absorption coefficient parameter increase, irrespective of the heated surface.
4) As the SHS and NSS are heated, the radiation parameter R lowers the temperature profile for both hybrid nanofluids.
5) When either NSS or SHS is heated, with an increase of heat generation parameter, both flow rate and bulk temperature will increase.
6) From the regression coefficients of skin friction, the t-test based on P-values shows that the magnetic parameter (P = 0.03418) and heat generation parameter (P = 0.00737) are statistically significant when SHS is heated, while the heat generation parameter (P = 0.03198) is statistically significant when NSS is heated. Similarly, for the Nusselt number, either of the surfaces is heated for hybrid nanofluid 1 and the radiation parameter R is statistically significant, and for hybrid nanofluid 2, the parameter heat generation parameter is statistically significant.
7) The magnetic parameter increases the velocity profile for both hybrid nanofluids when SHS and NSS are heated.

Acknowledgments: This project was supported by Researchers Supporting Project Number (RSP2024R411), King Saud University, Riyadh, Saudi Arabia.

Funding information: This project was supported by Researchers Supporting Project Number (RSP2024R411), King Saud University, Riyadh, Saudi Arabia.

Author contributions: All authors have accepted responsibility for the entire content of this manuscript and approved its submission.

Conflict of interest: The authors state no conflict of interest.

Data availability statement: The datasets generated and/or analyzed during the current study are available from the corresponding author on reasonable request.

References

[1] Lee S, Choi SUS, Li S, Eastman JA. Measuring thermal conductivity of fluids containing oxide nanoparticles. J Heat Transf. 1999;121(2):280–9. doi: 10.1115/1.2825978.
[2] Kuznetsov A, Nield D. The Cheng–Minkowycz problem for natural convective boundary layer flow in a porous medium saturated by a nanofluid: A revised model. Int J Heat Mass Transf. 2013;65:682–5. doi: 10.1016/j.ijheatmasstransfer.2013.06.054.
[3] Cheng P, Minkowycz WJ. Free convection about a vertical flat plate embedded in a porous medium with application to heat transfer from a dike. J Geophys Res. 1977;82(14):2040–4. doi: 10.1029/jb082i014p02040.
[4] Zainal NA, Nazar R, Naganthran K, Pop I. Viscous dissipation and MHD hybrid nanofluid flow towards an exponentially stretching/shrinking surface. Neural Comput Appl. 2021;33(17):11285–95. doi: 10.1007/s00521-020-05645-5.
[5] Rao AS, Ramaiah KD, Kotha G, Rao MVS, Chamkha AJ. A spectral relaxation approach for boundary layer flow of nanofluid past an exponentially stretching surface with variable suction in the presence of heat source/sink with viscous dissipation. Arab J Sci Eng. 2021;46(8):7509–20. doi: 10.1007/s13369-021-05422-z.

[6] Mandal IC, Mukhopadhyay S. Nonlinear convection in micropolar fluid flow past a non-isothermal exponentially permeable stretching sheet in presence of heat source/sink. Therm Eng. 2020;67(4):202–15. doi: 10.1134/s0040601520040059.

[7] Hussien AA, Al-Kouz W, Yusop NM, Abdullah MZ, Janvekar AA. A brief survey of preparation and heat transfer enhancement of hybrid nanofluids. Strojniški Vestn – J Mech Eng. 2019;65:441–53. doi: 10.5545/sv-jme.2019.6077.

[8] Junoh MM, Ali FM, Arifin NM, Bachok N, Pop I. MHD stagnation-point flow and heat transfer past a stretching/shrinking sheet in a hybrid nanofluid with induced magnetic field. Int J Numer Methods Heat Fluid Flow. 2019;30(3):1345–64. doi: 10.1108/hff-06-2019-0500.

[9] Subhani M, Nadeem S. Numerical analysis of micropolar hybrid nanofluid. Appl Nanosci. 2018;9(4):447–59. doi: 10.1007/s13204-018-0926-2.

[10] Sajjan K, Shah NA, Ahammad NA, Raju C, Kumar MD, Weera W. Nonlinear Boussinesq and Rosseland approximations on 3D flow in an interruption of Ternary nanoparticles with various shapes of densities and conductivity properties. AIMS Math. 2022;7(10):18416–49. doi: 10.3934/math.20221014.

[11] Raju C, Ahammad NA, Sajjan K, Shah NA, Yook SJ, Kumar MD. Nonlinear movements of axisymmetric ternary hybrid nanofluids in a thermally radiated expanding or contracting permeable Darcy Walls with different shapes and densities: Simple linear regression. Int Commun Heat Mass Transf. 2022;135:106110. doi: 10.1016/j.icheatmasstransfer.2022.106110.

[12] Sajjan K, Ahammad NA, Raju CSK, Prasad MK, Shah NA, Botmart T. Study of nonlinear thermal convection of ternary nanofluid within Darcy-Brinkman porous structure with time dependent heat source/sink. AIMS Math. 2023;8(2):4237–60. doi: 10.3934/math.2023211.

[13] Kumar MD, Raju C, Sajjan K, El-Zahar ER, Shah NA. Linear and quadratic convection on 3D flow with transpiration and hybrid nanoparticles. Int Commun Heat Mass Transf. 2022;134:105995. doi: 10.1016/j.icheatmasstransfer.2022.105995.

[14] Gireesha BJ, Umeshaiah M, Prasannakumara B, Shashikumar NS, Archana M. Impact of nonlinear thermal radiation on magnetohydrodynamic three dimensional boundary layer flow of Jeffrey nanofluid over a nonlinearly permeable stretching sheet. Phys A: Stat Mech Appl. 2020;549:124051. doi: 10.1016/j.physa.2019.124051.

[15] Nasir S, Islam S, Gul T, Shah Z, Khan MA, Khan W, et al. Three-dimensional rotating flow of MHD single wall carbon nanotubes over a stretching sheet in presence of thermal radiation. Appl Nanosci. 2018;8(6):1361–78. doi: 10.1007/s13204-018-0766-0.

[16] Ramesh G, Prasannakumara B, Gireesha B, Shehzad S, Abbasi F. Three dimensional flow of Maxwell fluid with suspended nanoparticles past a bidirectional porous stretching surface with thermal radiation. Therm Sci Eng Prog. 2017;1:6–14. doi: 10.1016/j.tsep.2017.02.006.

[17] Gireesha B, Archana M, Prasannakumara BC, Gorla RR, Makinde OD. MHD three dimensional double diffusive flow of Casson nanofluid with buoyancy forces and nonlinear thermal radiation over a stretching surface. Int J Numer Methods Heat Fluid Flow. 2017;27(12):2858–78. doi: 10.1108/hff-01-2017-0022.

[18] Besthapu P, Haq RU, Bandari S, Al-Mdallal QM. Thermal radiation and slip effects on MHD stagnation point flow of non-Newtonian nanofluid over a convective stretching surface. Neural Comput Appl. 2017;31(1):207–17. doi: 10.1007/s00521-017-2992-x.

[19] Chen CK, Weng HC. Developing natural convection with thermal creep in a vertical microchannel. J Phys D: Appl Phys. 2006;39(14):3107–18. doi: 10.1088/0022-3727/39/14/034.

[20] Davies J, Maynes D, Webb BW, Woolford B. Laminar flow in a microchannel with superhydrophobic walls exhibiting transverse ribs. Phys Fluids. 2006;18(8):087110. doi: 10.1063/1.2336453.

[21] Ng CO, Wang CY. Natural convection in a vertical microannulus with superhydrophobic slip and temperature jump. J Thermophys Heat Transf. 2014;28(2):287–94. doi: 10.2514/1.t4200.

[22] Jha BK, Gwandu BJ. MHD free convection in a vertical slit micro-channel with super-hydrophobic slip and temperature jump: non-linear Boussinesq approximation approach. SN Appl Sci. 2019;1(6):603. doi: 10.1007/s42452-019-0617-y.

[23] Bhatti MM, Zeeshan A. Analytic study of heat transfer with variable viscosity on solid particle motion in dusty Jeffery fluid. Mod Phys Lett B. 2016;30(16):1650196. doi: 10.1142/s0217984916501967.

[24] Krishna MV, Chamkha AJ. Hall effects on MHD squeezing flow of a water-based nanofluid between two parallel disks. J Porous Media. 2019;22(2):209–23. doi: 10.1615/jpormedia.2018028721.

[25] Krishna MV, Anand PVS, Chamkha AJ. Heat and mass transfer on free convective flow of amicropolar fluid through a porous surface with inclined magnetic field and Hall effects. Spec Top Rev Porous Media: Int J. 2019;10(3):203–23. doi: 10.1615/specialtopicsrevporousmedia.2018026943.

[26] Krishna MV, Swarnalathamma B, Chamkha AJ. Investigations of Soret, Joule and Hall effects on MHD rotating mixed convective flow past an infinite vertical porous plate. J Ocean Eng Sci. 2019;4(3):263–75. doi: 10.1016/j.joes.2019.05.002.

[27] Krishna MV, Chamkha AJ. Hall and ion slip effects on Unsteady MHD convective rotating flow of nanofluids – Application in biomedical engineering. J Egypt Math Soc. 2020;28(1):1. doi: 10.1186/s42787-019-0065-2.

[28] Krishna MV, Jyothi K, Chamkha AJ. Heat and mass transfer on MHD flow of second-grade fluid through porous medium over a semi-infinite vertical stretching sheet. J Porous Media. 2020;23(8):751–65. doi: 10.1615/jpormedia.2020023817.

[29] Krishna MV, Bharathi K, Chamkha AJ. Hall effects on MHD peristaltic flow of Jeffrey fluid through porous medium in a vertical stratum. Interfacial Phenom Heat Transf. 2018;6(3):253–68. doi: 10.1615/interfacphenomheattransfer.2019030215.

[30] Sajjan K, Raju CSK. Exact solutions of hydromagnetic convective flow in a microchannel with superhydrophobic slip and temperature jump: Microfluidics applications. Heat Transf. 2024;53(6):2749–92. doi: 10.1002/htj.23055.

[31] Zhang K, Raju C, Sajjan K, Almutairi B, Shah NA, Eldin SM. Nonlinear free convective with longitudinal slits in the presence of super-hydrophobic and non-hydrophobic microchannels in a suspension of nanoparticles: Multi-Linear Regression Analysis. Case Stud Therm Eng. 2023;49:103138. doi: 10.1016/j.csite.2023.103138.

Appendix

$$(Y, y, \lambda) = \frac{(x, y', \lambda')}{L}; \quad u = UU_0; \quad \theta = \frac{(T - T_0)}{(T_\mathrm{w} - T_0)};$$

$$\mathrm{Ec} = \frac{{U_0}^2}{(\rho_{\mathrm{Cp}})_\mathrm{f}(T_\mathrm{w} - T_0)}; \quad q_\mathrm{r} = -\frac{4\sigma^*}{3k^*}\frac{\mathrm{d}T^4}{\mathrm{d}y^4}; \quad \mathrm{Re} = \frac{L^2U_0}{k_\mathrm{f}};$$

$$M = B_0L\sqrt{\frac{\sigma_\mathrm{f}}{\rho_\mathrm{f}\nu_\mathrm{f}}}; \quad N = \left(\frac{\beta_1}{\beta_0}\right)_\mathrm{f}(T_\mathrm{w} - T_0); \quad \mathrm{Kp} = \frac{L}{\sqrt{\kappa}};$$

$$\mathrm{Pr} = \frac{\mu_\mathrm{f}(\rho_{\mathrm{Cp}})_\mathrm{f}}{k_\mathrm{f}}; \quad R = \frac{4\sigma^*{T_0}^3}{kk^*}; \quad Q_\mathrm{T} = \frac{L^2Q_0}{k_\mathrm{f}};$$

$$T^4 \cong 4{T_0}^3T - 3{T_0}^4;$$